Water Air Soil Pollut (2012) 223:5817–5840
DOI 10.1007/s11270-012-1319-x

Prediction of Vertical DNAPL Vapour Fluxes in Soils Using Quasi-Analytical Approaches: Bias Related to Density-Driven and Pressure-Gradient-Induced Advection

Salsabil Marzougui · Gerhard Schäfer · Lotfi Dridi

Received: 28 April 2012 / Accepted: 6 September 2012 / Published online: 29 September 2012

Abstract This study focuses on a detailed analysis of the errors introduced by two quasi-analytical approaches based on either Fick's first law or a combination of Fick's and Darcy's laws to evaluate the vapour flux of chlorinated solvents from a source zone located in the unsaturated zone towards the atmosphere. A coupled one-dimensional numerical flow and transport model was developed and applied to three case studies characterised by different water content profiles in the vadose zone and under different levels of maximum dense nonaqueous-phase liquid vapour concentrations and vapour pressure conditions of the source zone. The steady-state concentration and pressure profiles obtained were then used in the two quasi-analytical approaches to estimate the flux towards the atmosphere. When mass fluxes due to density-driven advection become dominant and the vertical advective mass fluxes are increased due to strong pressure gradients in the soil air, the error was observed to increase when using the pure diffusion approach in the quantification of the surface flux calculated by the numerical model with increasing dimensionless Rayleigh numbers. Without taking into account the advective transport in the approach, the relative error calculated with only Fick's law overestimates the real vapour flux when density-driven advection is dominant and underestimates it when pressure-gradient-driven advection dominates. The more advanced advective–diffusive quasi-analytical approach fits reasonably well with the numerically obtained mass fluxes except near soil layer discontinuities, where the evaluation of both the concentration gradient and pressure gradient in the porous media as well as the determination of the average effective diffusion coefficients are rendered more difficult.

Keywords DNAPL vapour flux · Density-driven advection · Pressure-gradient-induced advection · Quasi-analytical approach · Soil pollution · Vadose zone

S. Marzougui · G. Schäfer (✉)
Laboratoire d'Hydrologie et de Géochimie de Strasbourg,
UMR 7517 CNRS-Université de Strasbourg,
1 rue Blessig,
67084 Strasbourg Cedex, France
e-mail: schafer@unistra.fr

L. Dridi
Institut Supérieur Agronomique de Chott Meriem (ISA-CM),
BP47, 4042, Chott Meriem,
Sousse, Tunisia

1 Introduction

Spills and leaks of so-called dense nonaqueous-phase liquids (DNAPLs), such as trichloroethylene (TCE), commonly used for many years in the industry have severely impacted the quality of subsurface water supplies (Kueper and Frind 1989; Birovljev et al. 1991; Fayers and Zhou 1996; Bettahar et al. 1999; Benremita and Schäfer 2003; Bohy et al. 2004; Dridi et al. 2009). In the subsurface, DNAPLs migrate

vertically depending upon gravity and capillary forces through the unsaturated zone. Because of their high volatility, a large vapour plume appears to form a plume of pollution (Falta et al. 1989). These vapours can migrate by advection–diffusion from the unsaturated zone to the groundwater (Mendoza and McAlary 1990; Jones et al. 1978; Jellali et al. 2003; Cotel et al. 2011) or can be transferred from the soil surface to the atmosphere and indoor air of buildings (Hodgson et al. 1992; Johnson and Ettinger 1991; Morisson et al. 2006; Yu et al. 2009).

Today, one of the key challenges in the remediation of contaminated sites is accurately predicting the environmental impact of organic pollution caused by DNAPL in terms of vapour concentrations in the soil gas of the vadose zone, in the atmosphere close to the soil surface and in the indoor air of overlaying buildings. To better understand the behaviour of volatile organic compound (VOC) vapours in the soil gas, a study of the source zone is necessary. Several studies have investigated different aspects of this issue. A large number of numerical studies have been conducted in the past (e.g. Sleep and Sykes 1989; Thomson et al. 1997; Jang and Aral 2007; White et al. 2008; Coppola et al. 2009; Molins et al. 2010) to quantify the attenuation of the source zone of pollution being caused by phase partitioning, biodegradation of VOCs and change of soil–air pressure and/or temperature change. Only a few controlled laboratory experiments investigated the attenuation of the source zone (Jones et al. 1978; Sililo and Tellam 2000). Kram et al. (2001) described screening methods and approaches used to detect and delineate DNAPL contaminant source zones. Mass partitioning between the different fluid phases (DNAPL, water and gas) and the solid matrix has been discussed in many studies. For example, Mendoza and Frind (1990), Jellali et al. (2003), Bohy et al. (2006) and Cotel et al. (2011) assessed the liquid–gas partioning using Henry's law in their experimental studies. However, the most important transport mechanisms of DNAPL in unsaturated porous media are diffusion and advection.

Diffusion is considered as the predominant transport mechanism for vapours in the unsaturated zone and is often assessed using Fick's first law (Pankow and Cherry 1996; Choi et al. 2002; Webb and Pruess 2003; Jellali et al. 2003; Bohy et al. 2006; Cotel 2008). However, in natural soils, advective transport of DNAPL vapours might become significant; this transport can be generated by density gradients that exist within and along the fringe of the vapour plume or by pressure gradients in the gas phase. The effects of density-induced transport have been investigated in a large number of numerical modelling studies (e.g. Sleep and Sykes 1989; Falta et al. 1989; Mendoza and Frind 1990; Mendoza and McAlary 1990; Lenhard et al. 1995; Mastrocicco et al. 2011). These studies demonstrate that density-induced advection can be a significant transport mechanism and mainly depends on the permeability of the medium, the thickness of the unsaturated zone and the temperature of the soil. Only a few experiments have been conducted to study the VOC vapour density effect (e.g. Schwille, 1988; Lenhard et al. 1995; Altevogt et al. 2003; Jang and Aral 2007; Cotel et al. 2011).

Pressure gradients in the soil gas may provoke a driving pressure field, resulting in pressure-induced advection of the vapour concentrations. For an isotropic porous medium, vapour migration along the given pressure gradient may therefore be more spatially extended in the unsaturated zone than by the effect of diffusive transport alone. Pressure gradients are usually driven by barometric pressure variations, by vaporisation of the DNAPL at the source zone and ventilated buildings or by the movement of water in the unsaturated zone (Barber et al. 1990; Parker 2003; Williams et al. 1999; Altevogt et al. 2003; Mendoza and Frind 1990; Rivett et al. 2011).

As subsurface pollution by VOCs represents a serious environmental problem in many industrial areas (DRSP 2007), mathematical vapour transport models are employed to evaluate the health risk caused by the inhalation of polluted vapours at contaminated sites. However, the main tools actually used in field applications are quasi-analytical solutions and are commonly based on diffusive vapour transport (Jellali et al. 2003; Bohy et al. 2006; Dridi and Schäfer 2006) without taking into account the influence of the density of the DNAPL vapours and the pressure gradient in the soil gas. Only a few models, such as the VOLASOIL model (Waitz et al. 1996) and the Johnson and Ettinger model (Johnson and Ettinger 1991), currently used by engineering companies as tools for quantifying mass fluxes from the subsurface to the atmosphere account for both the diffusive and advective transport of DNAPL vapours. However, these models do not explicitly distinguish between density-driven advection and pressure-gradient-induced advection. Indeed, this deficiency can lead to high uncertainties in the

prediction of vapour fluxes that renders an appropriate estimation of the health risk difficult.

This study focuses on a detailed error analysis when evaluating DNAPL vapour fluxes at the soil surface using quasi-analytical solutions. Two modelling approaches are used: the first one is based only on Fick's first law of diffusion, and the second takes into account diffusion, dispersion and advection of DNAPL vapour fluxes. To build up a solid database of vertical profiles of vapour concentration and soil pressure, we used a coupled one-dimensional (1D) numerical flow and transport model to calculate vapour fluxes from a DNAPL source zone located in the vadose zone towards the atmosphere. In three case studies, the modelling area comprises an unsaturated soil column of 1-m height with different soil texture at different water contents. The lower boundary condition represents the source zone and is defined by a prescribed vapour pressure and concentration.

Under steady-state transport conditions, we compare the vapour fluxes calculated at the upper boundary of the soil column with the 1D numerical model to the vapour fluxes quantified between two depths of the soil column, where one of them is located at the soil/atmosphere interface using two quasi-analytical approaches. The first approach is based on Fick's first law of diffusion; it estimates the vertical mass flux per unit surface towards the atmosphere using the numerically calculated concentration data at a given time. Three input terms are required in this approach: the measured concentration difference between two measuring points, their vertical distance and the average effective diffusion coefficient between the two depths.

The second approach takes into account the vapour density term and the effect of pressure gradients, is based on both Fick's and Darcy's laws and quantifies the total vertical (advective, diffusive and dispersive) mass flux per unit surface towards the soil surface. This approach depends on the effective coefficient of gas diffusion, the DNAPL vapour density as a function of the measured vapour concentration and the monitored vapour pressure and concentration at two different depths.

To analyse in detail the bias introduced by each of the two quasi-analytical approaches, a relative error is defined between the vapour flux obtained from the quasi-analytical approaches and the numerically calculated flux at the upper boundary of the soil column.

2 Mathematical Tool

To model the 1D vapour transport in a soil column, a mathematical approach was used that is based on a coupled flow and transport model for the gas phase in the given three-phase (water–gas-porous medium) system.

2.1 Flow Model

Considering the DNAPL vapour as a gas mixture of the uncontaminated soil gas and the vaporised DNAPL, the gas flow in the vertical z-direction in a partially saturated porous medium is described by the mass conservation equation:

$$-\frac{\partial}{\partial z}(\rho v) = \frac{\partial(\theta_g \rho)}{\partial t} \tag{1}$$

where ρ (in kilogrammes per cubic metre) is the vapour or gas density, v (in metres per second) is Darcy's velocity in the z-direction or the specific discharge of the gas phase and θ_g (−) is the gas content of the porous medium.

Assuming the ideal gas law, the gas density can be expressed as follows:

$$\rho(p,T) = \frac{pM}{RT} \tag{2}$$

where M (in kilogrammes per mole) is the molecular weight of the gas, p (in Pascals) is the gas pressure, R (8.314 Pa $m^3 mol^{-1} K^{-1}$) is the universal ideal gas constant and T (in Kelvins) is the absolute temperature.

The generalised Darcy's law (Bear 1972) expresses the specific discharge of the gas phase

$$v = -\frac{k}{\mu}\frac{\partial}{\partial z}(\rho g z + p) \tag{3}$$

where k (in square metres) is the gas permeability, g (in metres per square second) is the gravity acceleration, μ (in kilogrammes per metre per second) is the dynamic viscosity of fluid and z (in metres) is the elevation.

In the given flow model, the gas permeability of the porous medium is given by

$$k = k^* k_{ra} = k^* \left(\frac{S_g}{1 - S_{wr}}\right)^3 \tag{4}$$

where k^* (in square metres) is the intrinsic permeability and k_{ra} (−) is the relative permeability function of

the gas saturation (S_g (−)) and the irreducible water saturation (S_{wr} (−)).

Introducing Eqs. (2) and (3) into Eq. (1) and after some development (see Appendix A), the mass conservation equation can be written as

$$\frac{\theta_g M}{RT}\frac{\partial p}{\partial t} = \frac{M^2 g}{\mu R^2 T^2}\frac{\partial}{\partial z}\left(kp^2\right) + \frac{M}{2\mu RT}\frac{\partial}{\partial z} \times \left(k\frac{\partial p^2}{\partial z}\right) \quad (5)$$

Equation (5) can be linearised by rewriting p^2 in the storage term as

$$\frac{\partial p^2}{\partial t} = \frac{\partial (pp)}{\partial t} = p\frac{\partial p}{\partial t} + p\frac{\partial p}{\partial t} = 2p\frac{\partial p}{\partial t} \quad (6)$$

Replacing $\frac{\partial p}{\partial t}$ with $\frac{1}{2}\frac{\partial p^2}{p\,\partial t}$ leads to

$$\frac{\partial p^2}{\partial t} = \frac{p}{\mu\theta_g}\frac{\partial}{\partial z}\left(k\frac{\partial p^2}{\partial z}\right) + 2\frac{Mgp}{\mu RT\theta_g}\frac{\partial}{\partial z}\left(kp^2\right) \quad (7)$$

The final linearised flow equation is obtained by replacing p^2 by P:

$$\frac{\partial P}{\partial t} = \beta\frac{\partial}{\partial z}\left(k\frac{\partial P}{\partial z}\right) + 2\gamma\frac{\partial}{\partial z}(kP) \quad (8)$$

where

$$\beta = \frac{p_0}{\mu\theta_g}\,;\gamma = \frac{Mgp}{\mu RT\theta_g}$$

and p_0 represents the initial pressure.

The molecular weight of the vapour M (in kilogrammes per mole) depends on the vapour concentration C (in kilogrammes per cubic metre) in the gas mixture and is calculated by the model using the following equation (Thomson et al. 1997):

$$M = C\frac{RT}{p}\left(1 - \frac{M_{air}}{M_{DNAPL}}\right) + M_{air} \quad (9)$$

where M_{air} (in kilogrammes per mole) and M_{DNAPL} (in kilogrammes per mole) represent the molecular weights of the uncontaminated soil air and the DNAPL, respectively.

2.2 Transport Model

Let us consider vapour transport in a partially saturated porous medium. The transport equation in the vertical z-direction can be written using the classical advection–diffusion–dispersion equation commonly employed in unsaturated porous media:

$$\alpha\frac{\partial C}{\partial t} = \frac{\partial}{\partial z}\left(\left(D_{eg} + \alpha_L|v|\right)\frac{\partial C}{\partial z}\right) - \frac{\partial}{\partial z}(vC) \quad (10)$$

where C (in kilogrammes per cubic metre) denotes the vapour concentration, D_{eg} (in square metres per second) denotes the effective diffusion coefficient of the gas phase, and α_L (in metres) denotes the longitudinal dispersivity of the porous medium. α represents the capacity factor of the porous medium and is expressed by

$$\alpha = \theta_g + \frac{\theta_w}{H} \quad (11)$$

where θ_g (−) denotes the gas content in the soil air, θ_w (−) is the water content and H (−) is the Henry constant.

D_{eg} is assumed to be time invariant. The mathematical formulation of the effective diffusion coefficient is given by (Grathwohl 1998; Wang et al. 2003)

$$D_{eg} = \theta_g\,\tau\,D_g \quad (12)$$

where τ (−) represents the tortuosity of the porous medium and is based on the Penman–Millington Quirk model (Moldrup et al. 1997):

$$\tau = 0.66\frac{\theta_g}{n} \quad (13)$$

where D_g (in square metres per second) is the free-air diffusion coefficient and n (−) is the porosity of the porous medium.

The vapour velocity v is given by Darcy's law (see Eq. 3).

2.3 Numerical Flow and Transport Model

The method used to numerically solve Eqs. (8) and (10) is the finite volume method. The study area is a 1D domain discretised into N cells, where k represents the centre of the cell, $k-1/2$ is the upstream cell edge and $k+1/2$ is the downstream cell edge. The integral of the linearised flow equation (Eq. 8) and transport equation (Eq. 10) are described in detail in Appendix B.

The parameters C, α, α_L, β, γ and P are defined in the centre of the cell, whereas v, the gas permeability k and θ_g are defined at the cell edges.

To solve the coupled system of equations, a Picard linearisation is used. The 1D model uses a dataset containing constants and parameters necessary to

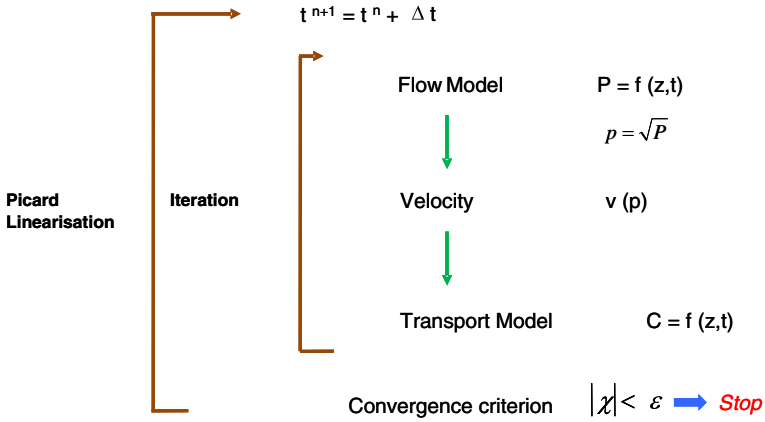

Fig. 1 Progress of computation

solve the equations, such as the number of cells and edges, time step, intrinsic permeability, β, γ, M, θ_g, S_{wr} and the initial conditions of the vapour concentrations and pressures.

First, the model calculates the pressure from the flow model in which it uses the β, γ and M given in the data file. Once the pressure is determined, it will be used to calculate Darcy's velocity v. This velocity will be used in the transport model to compute the vapour concentration in the centre of each cell.

Before starting the next time step, the model calculates the new χ (new beta (β_{new}), new gamma (γ_{new}) and a new molecular weight (M_{new})) to calculate the pressure. These new entries χ should not deviate significantly from the old values β_{old}, γ_{old} and M_{old}. Therefore, a convergence condition is used: the absolute value of the relative differences $\left|\frac{\chi_{new}-\chi_{old}}{\chi_{old}}\right|$ should not exceed the convergence criterion of 10^{-11}. If this criterion is not achieved, the model recalculates these entries in a further loop called L_{iter} (Fig. 1) until this criterion is met. The numerical model then proceeds with the next time step. For each time step, the outputs of the numerical model are vapour concentration C, velocity v, pressure p, vapour fluxes and the effective diffusion coefficient D_{eg}.

3 Case Studies

3.1 Characteristics of Porous Media

Three different structures are used for the studied soil columns to qualitatively represent configurations of soil columns that are typically observed on real sites. Two sands are used: a fine sand (sand 1) and a medium-sized sand (sand 2). In the first case study A, the soil column is divided into two 50-cm thick layers in the vertical z-direction: the lower layer is formed by sand 2 and the upper one is composed of sand 1. The second case study uses a homogeneous configuration formed by sand 2 denoted as case study B. The soil structure of case study C is the inverse of case A (Fig. 2). The properties of the sands used are provided in Table 1. The DNAPL used in the case studies is TCE. Table 2 summarises the physical and chemical properties of TCE at 20 °C.

Numerical flow and transport modelling of TCE vapour is performed on a 1-m-high column, equally discretised in the vertical z-direction into 200-grid cells of Δz=0.005 m. The boundary conditions and the water content in the unsaturated soils are discussed in the following section.

3.2 Water Content and Effective Diffusion Coefficient

The various studies are performed using the 1D coupled numerical flow and transport model to produce

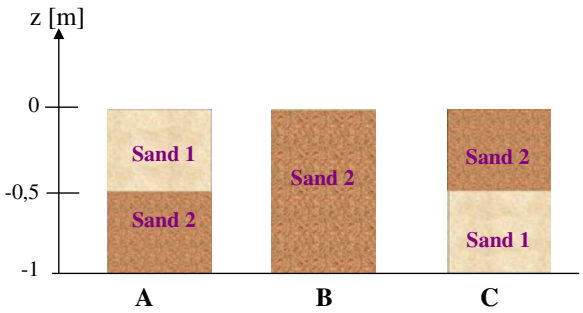

Fig. 2 Schematic representation of the three case studies

Table 1 Properties of the sand

Properties	Sand 1	Sand 2
Porosity (n (−))	0.43	0.4
Irreducible water saturation (S_{wr} (−))	0.17	0.15
Van Genuchten parameters		
α_{vg} (m^{-1})	0.0101	0.145
n_{vg} (−)	13	2.68
Intrinsic permeability (k^* (m^2))	5.1×10^{-12}	8.2×10^{-11}
Longitudinal dispersivity (α_L(m))	0.5×10^{-3}	1×10^{-3} (Benremita 2002)

the database of vertical profiles of DNAPL pressure and concentration in partially water-saturated porous media. Figure 3 presents the steady-state water content profiles of the different case studies obtained from Dridi and Schäfer (2006) using the multiphase flow simulator SIMUSCOPP (Thiez and Ducreux 1994). Case B is characterised by a constant water content of 0.06, whereas in case A, a perched water table is observed. In case C, a high jump in water content is observed at the discontinuity between the two layers of sand. Using Eq. (12), the effective gas diffusion coefficients are obtained from the given water content profiles (Fig. 3b).

3.3 Initial and Boundary Conditions

The initial conditions and boundary conditions selected in the numerical case studies are provided in Fig. 4. Initially, the soil gas within the entire soil column is assumed to be uncontaminated (C=0), and its pressure increases with depth, corresponding to an ideal gas at static equilibrium expressed by an exponential law. At the upper boundary of the soil column (z=0 m) corresponding to the soil surface, the pressure and concentration of the TCE vapours are prescribed and fixed at a constant value. In all studies, the gas pressure is equal to an atmospheric pressure of 1 atm, and the vapour concentration (denoted $C_{downstream}$) is assumed to be zero. At the upstream boundary corresponding to the lower end of the soil column (z=−1 m), the vapour concentration and gas pressure are defined for the different runs of each case study (Table 3). Three modes of transport of TCE vapours are simulated in the soil columns: (1) purely diffusive transport (Run 3), (2) transport of vapours with density effect (Run 1) and (3) transport of vapours under the combined effect of vapour density and pressure gradients (Runs 4, 6, 7, 9 and 11). The case of purely diffusive transport has been studied in the paper of Dridi and Schäfer (2006), where they demonstrated that in the case of purely diffusive transport, steady-state conditions are reached after 5 days, and the heterogeneity of the porous medium has a significant effect on vapour transport in the soil column. For example in case B, the steady-state TCE vapour concentration was characterised by a linear profile due to the constant effective diffusion coefficient. However, in case A, the concentrations were lower at the top of the soil column than for the homogeneous medium, caused by the effect of the low effective gas diffusion coefficients of the upper layer formed by sand 1. Therefore, the TCE vapour concentrations in sand 2 were higher than the vapour concentration for the homogeneous media because of the diffusion barrier generated by sand 1. While for case C, the vapour flux from the source to the atmosphere was lower than in case B, it was higher than in case A. Indeed, this result arose from the high water content in the lower layer.

In our study, we focus on the case of transport under the influence of vapour density and driving pressure p_g (in Pascals), defined as $p_g=p+\rho gz$.

Table 2 Physical and chemical properties of trichloroethylene at 20 °C

Molecular diffusion coefficient in free air (D_g (m^2/s))	7.4×10^{-6} (Perry and Green 1984)
Henry constant (H (−))	0.229 (Nordstrom and Munoz 1985)
Molecular weight (g/mol)	131.39
Vapour pressure at saturation (p_v (Pa))	4,475
Vapour concentration at saturation C_{sat} (kg/m^3)	0.25

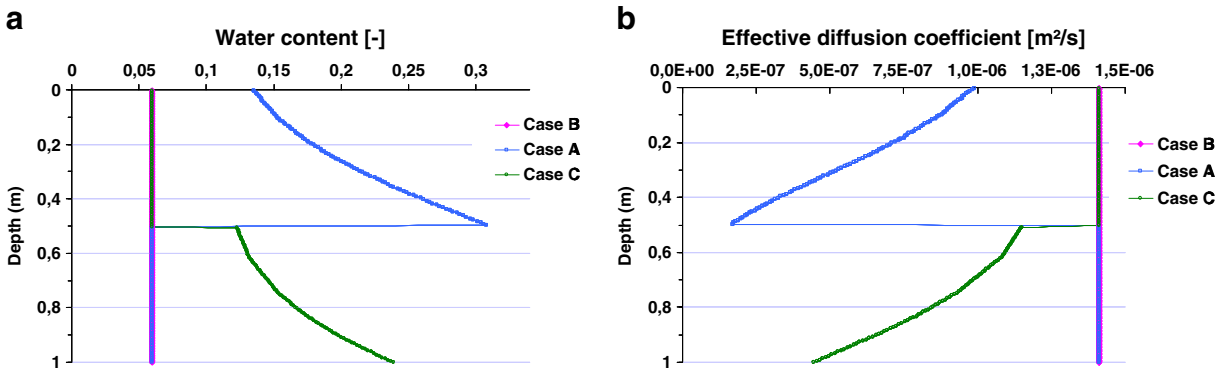

Fig. 3 Water content and effective diffusion coefficient as a function of depth used in the three case studies (Dridi and Schäfer 2006)

In the upstream boundary, the TCE vapour concentration of the source zone is assumed to be time invariant. The maximum vapour concentration of the TCE is C_{upstream}=0.25 kg/m^3, and its maximum vapour pressure of p_v is equal to 4,475 Pa. Different levels of TCE vapour concentration and pressure are applied at the upstream boundary (at z=−1 m) (Table 3). The numerical flow and transport model (see Section 2) was used to calculate the transport of a VOC from the lower boundary of the unsaturated soil column (with a fixed concentration in the gas phase C_{upstream} and a fixed gas pressure) to the soil surface. In the following, the soil depth $\bar{z}(\bar{z} = -z)$ is used instead of elevation z.

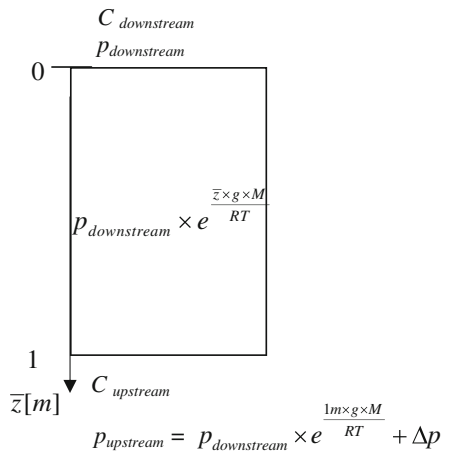

Fig. 4 Initial conditions and boundary conditions (Note: $\bar{z} = -z$)

3.4 Calculated DNAPL Vapour Concentration and Pressure Profiles and Vapour Fluxes

3.4.1 Influence of Density-Driven Advection

Figure 5 presents the vapour concentrations calculated in the soil column under transient and steady-state conditions for Run 1. For a homogeneous porous medium (case B), steady-state transport conditions are already achieved after 1.5 days. At this point, the vapour plume stagnates at the bottom of the soil column. This accumulation is mainly due to the effect of vapour density on vertical flow components, resulting in gravity-driven movement of the vapour. Indeed, as the concentrations at the lower part of the soil column are high, the density of the gas mixture is increased, achieving a maximum vapour density of approximately 1.34 kg/m^3 at the bottom of the column.

Table 3 Upstream boundary conditions selected for the different runs

	C_{upstream}			
	C_{sat}	$C_{\text{sat}}\times0.1$	$C_{\text{sat}}\times0.01$	$C_{\text{sat}}\times0.001$
Δp				
0	Run 1[a]	Run 2[a]	Run 3[a]	
$p_v\times0.001$	Run 4[a]	Run 5		Run 6[a]
$p_v\times0.01$	Run 7[a]	Run 8	Run 9[a]	
$p_v\times0.1$	Run 10	Run 11[a]		
p_v	Run 12			

[a] Data correspond to the runs discussed in detail in the text

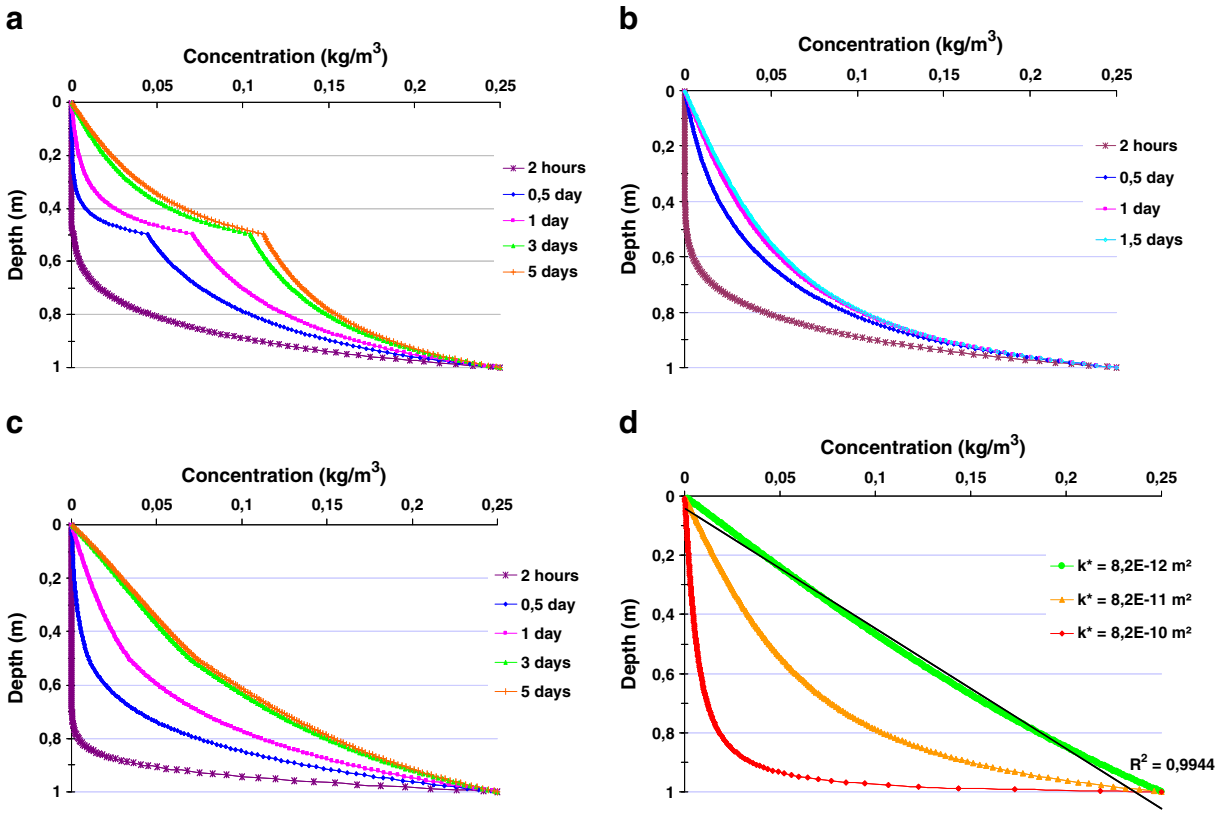

Fig. 5 Influence of vapour density on TCE vapour concentrations (Run 1): transient concentration profiles in the soil columns for **a** cases A, **b** B and **c** C and **d** concentration profile at steady state obtained for case B compared with those of two homogeneous media with different intrinsic permeabilities

The hydraulic conductivity of the porous medium may have a significant influence on density-driven advection of vapour, expressed by the dimensionless Rayleigh number (Cotel et al. 2011). The higher the intrinsic permeability, the higher the Rayleigh number and the density effect will be. In case A, the upper layer formed by fine sand 1 is less permeable than sand 2 located below.

In this case, the vapour concentrations in the upper layer are higher than in the homogeneous case (case B). To study the influence of the dimensionless Rayleigh number on the vertical concentration profile of TCE vapours, we varied the intrinsic permeability of the homogeneous medium on the steady-state concentration profile by dividing the initial value by ten and one tenth (Fig. 5d). When decreasing the intrinsic permeability to 8.2E−12 m^2, the vapour concentration profile has a linear form (R^2=0.994), which implies that the transport of the vapour plume is dominated by molecular diffusion (Dridi and Schäfer 2006). In this case, advective mass fluxes induced by the vapour density are negligibly small. However, for an increased intrinsic permeability of 8.2E−10 m^2, the vapour plume stagnates at the lower part (the first 10 cm) of the soil column.

For the heterogeneous porous medium of case C (Fig. 5c), the low permeability of the lower layer of the soil column causes the lower density-induced advective flux compared with case A (Fig. 5a, c). The diffusive, dispersive, advective and total vertical vapour fluxes obtained are plotted in Fig. 6. Note that the absolute values of the dispersive fluxes are very small compared with those of the diffusive and advective fluxes.

In case study C, the advective flux becomes positive in the upper part of the soil column (Fig. 6c). Hence, the vapours are dominated by an upward movement towards the soil surface caused by a decreasing driving pressure with increasing elevation z in medium-sized sand 2 (Fig. 6d). Compared with

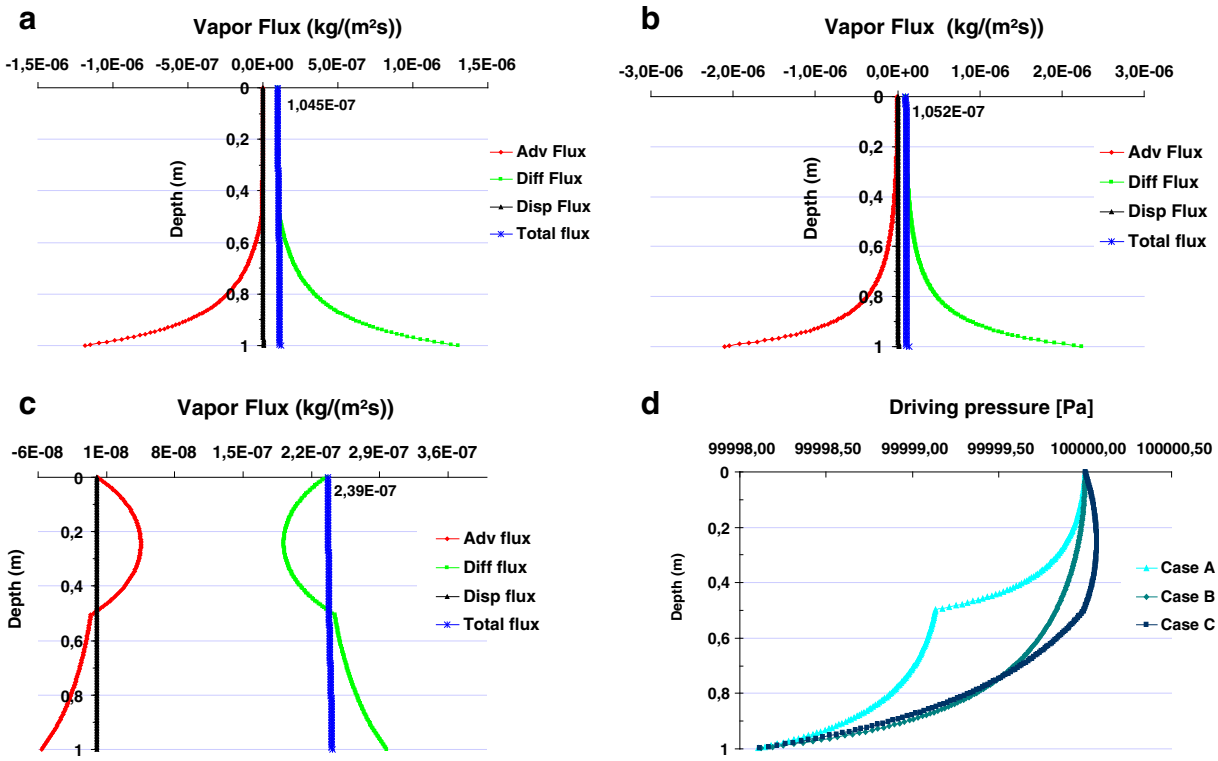

Fig. 6 Diffusive, dispersive, advective and total fluxes in *z*-direction calculated in Run 1 at steady state for **a** cases A, **b** B and **c** C, and **d** driving pressure calculated at steady state in Run 1 for cases A, B and C

case study B, where the driving pressure gradient near the soil surface is almost zero, the density-driven advective fluxes are very low near the soil surface. The effect of vapour density becomes negligible when approaching the soil surface of case study B (Fig. 6b). As in the lower part of the homogeneous sand filling (case B), the vapour density effect is the predominant transport parameter and the downwards orientated advective vapour flux is the highest calculated vapour flux.

However, as the vapour density effect of case study C is less significant, molecular gas diffusion becomes the dominant transport mechanism. Therefore, the total vapour flux calculated in case study C is higher than those of cases A and B (Fig. 6c).

Although the influence of vapour density on advective vapour flux strongly depends on the soil texture, it also depends on the prescribed upstream concentration boundary conditions. Figure 7 represents the normalised steady-state vapour concentration calculated for Runs 1, 2 and 3 as a function of depth; C_{upstream} corresponds to the TCE concentration prescribed at the upstream boundary of the soil column. Significantly reducing the prescribed vapour concentration may correspond to the field case where the source of pollution is far away from the considered location. Vapour fluxes resulting from density-driven advection become negligible, and the vapour plume is mainly governed by diffusive mass transport. In this case, the vertical concentration profiles correspond to those determined by Dridi and Schäfer (2006).

3.4.2 Combined Influence of Density-Driven and Pressure-Gradient-Induced Advection

Compared with Run 1, a slight overpressure $\Delta p = p_v \times 0.001$ is added in Run 4, representing a configuration where the observation point is located closely above the source zone. Vaporisation of the present DNAPL causes both an overpressure in the gas mixture and high vapour concentrations in the neighbourhood of the source zone. This phenomenon may result in advective vapour fluxes caused by both the gradient of

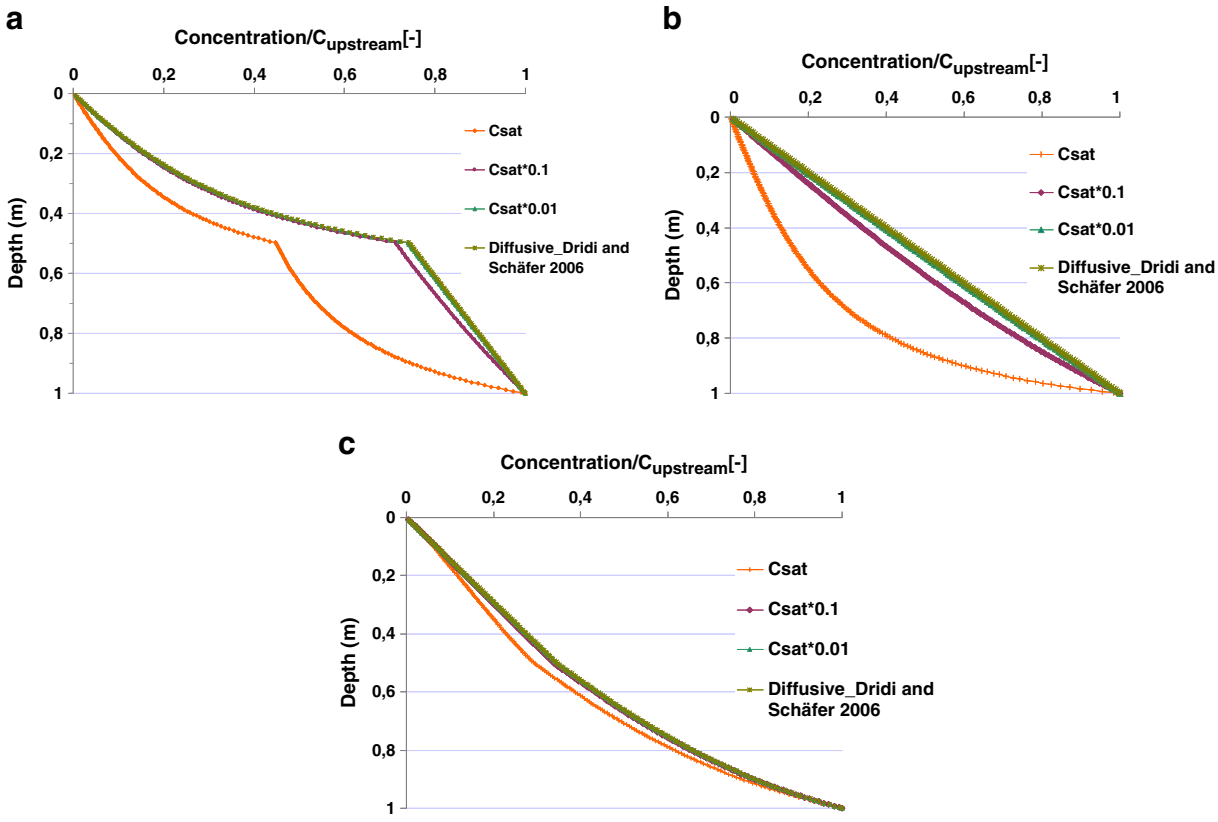

Fig. 7 Normalised TCE vapour concentration in the column calculated at steady state in Runs 1, 2 and 3 for different prescribed upstream boundary concentrations for **a** cases A, **b** B and **c** C

driving pressure and density effects. In the following section, the combined influence of the prescribed concentration and pressure condition at the upstream boundary on the vertical vapour flux is studied. The results of Run 4 are plotted in Fig. 8. At the steady-state transport conditions of case study B, nearly 90 % of the total height of the soil column contains more than 50 % of the vapour concentration prescribed at the upstream boundary of the soil column after only 2 days (Fig. 8b).

Compared with Fig. 5, where the normalised vapour concentration of 0.5 does not exceed 10 cm of height, this may clearly be attributed to the pressure-gradient-induced advective flux that dominates the density-driven advective and diffusive fluxes. The diffusive, dispersive, advective and total vertical vapour fluxes obtained are plotted in Fig. 9. Note that the absolute values of the dispersive fluxes are very small compared with those of the diffusive and advection fluxes. The vapour pressure prescribed at the lower boundary of the soil column generates an ascendant movement of the TCE vapours, enhancing the saturation of the soil column with TCE vapours. This fact is underlined by the calculated vertical advective fluxes, which are positive and higher than the diffusive fluxes up to a depth of 10 cm (Fig. 9b). The corresponding driving pressure profile (Fig. 9d) confirms that an ascendant movement occurs over almost the entire column. Only for depths lower than 10 cm are the diffusive fluxes higher than the advective fluxes. The calculated total vapour flux is approximately 28 times higher than that of Run 1, where only the vapour density effect was taken into account.

The heterogeneity of the porous medium significantly affects the time to reach steady-state transport conditions (Fig. 8a, c). It exceeds 6 days for case study C, corresponding to three times the time required in the studied homogeneous medium (case B). The steady-state transport conditions are achieved in case A after 5 days. In case B, the total vapour flux is approximately 10 times higher than that of case C and 20 times higher than that of case A (Fig. 9).

The vapour concentration profiles calculated in case study A are similar to those obtained in the case

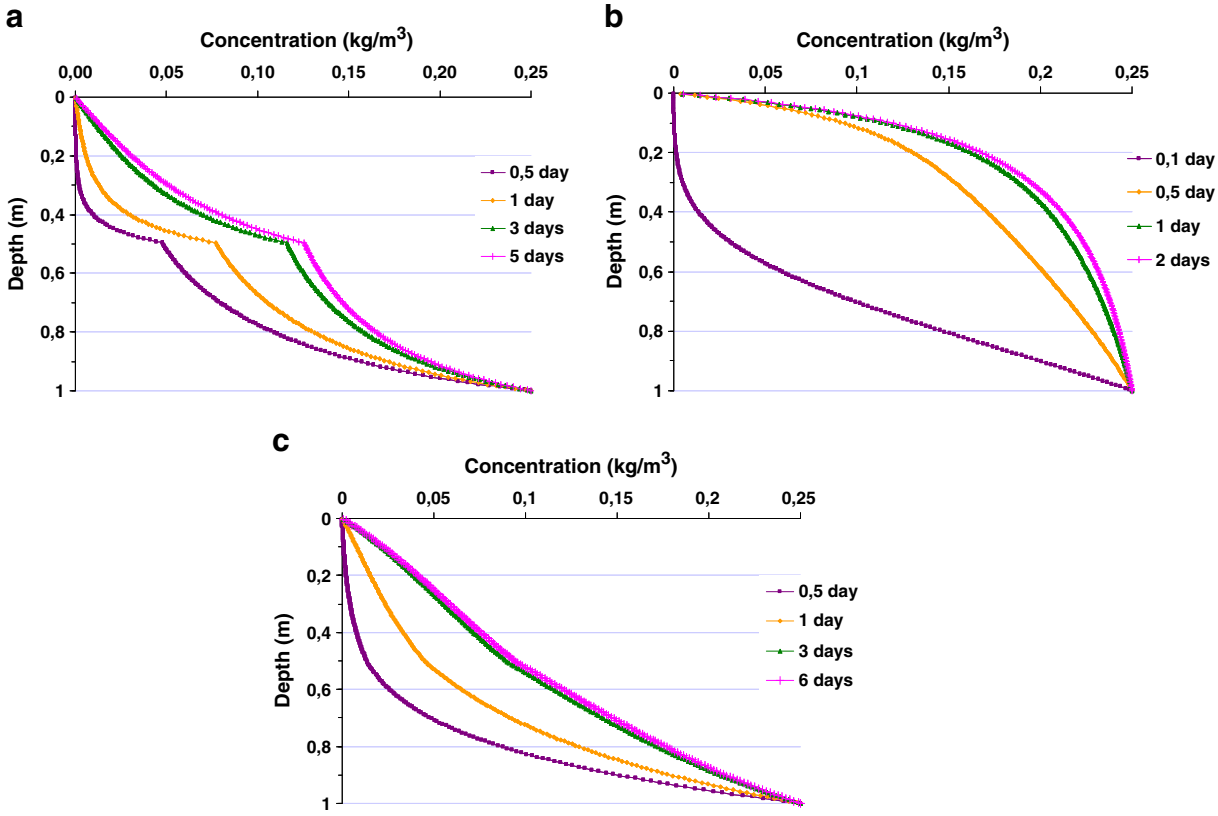

Fig. 8 TCE vapour concentration calculated in Run 4 for **a** cases A, **b** B and **c** C

of pure vapour density-induced advection (see Run 1). The selected slight overpressure at the upstream boundary does not have a significant influence on the vapour transport in the vertical direction. This fact is underlined by the calculated advective fluxes caused by both the vapour density effect and the vapour pressure gradient, which are in total negative up to a height of 40 cm (Fig. 9a). At smaller depths, they become positive but remain small. Compared with the case of the purely density-driven advective transport (Run 1), the calculated total flux is now 38 % higher.

For the results of Run 4 in case study C, the advective vapour fluxes are positive throughout the entire column. In this case, the effect of vapour density is negligible. Furthermore, the calculated total vapour flux is 50 % higher than the total flux in the case of Run 1, which implies that advective vapour transport in the vertical direction due to vapour pressure gradients is overcoming that caused by the density differences in the soil gas.

As observed in Table 3, different cases of concentration and pressure boundary conditions were studied. Figure 10 presents the results of Runs 4, 6, 7, 9 and 11 at steady-state transport conditions in comparison with the results of Runs 1 and 3 to analyse the effect of overpressure at the upstream boundary of the soil column.

Run 11 corresponds to the highest vapour pressure and vapour concentration prescribed at the lower boundary of the soil column (see Table 3). The transient vapour flux calculated at the soil surface is plotted in Fig. 10d for the case studies. The total flux calculated for case study B is approximately 20 times and 50 times higher than that determined for case studies C and A, respectively. To reach steady-state transport conditions, the time required is significantly shorter for case study B than for the two other case studies, as soil heterogeneity has a strong effect on vapour migration in case studies A and C.

Run 11 leads to the highest vapour concentration in the different soil configurations (Fig. 10a–c). Due to

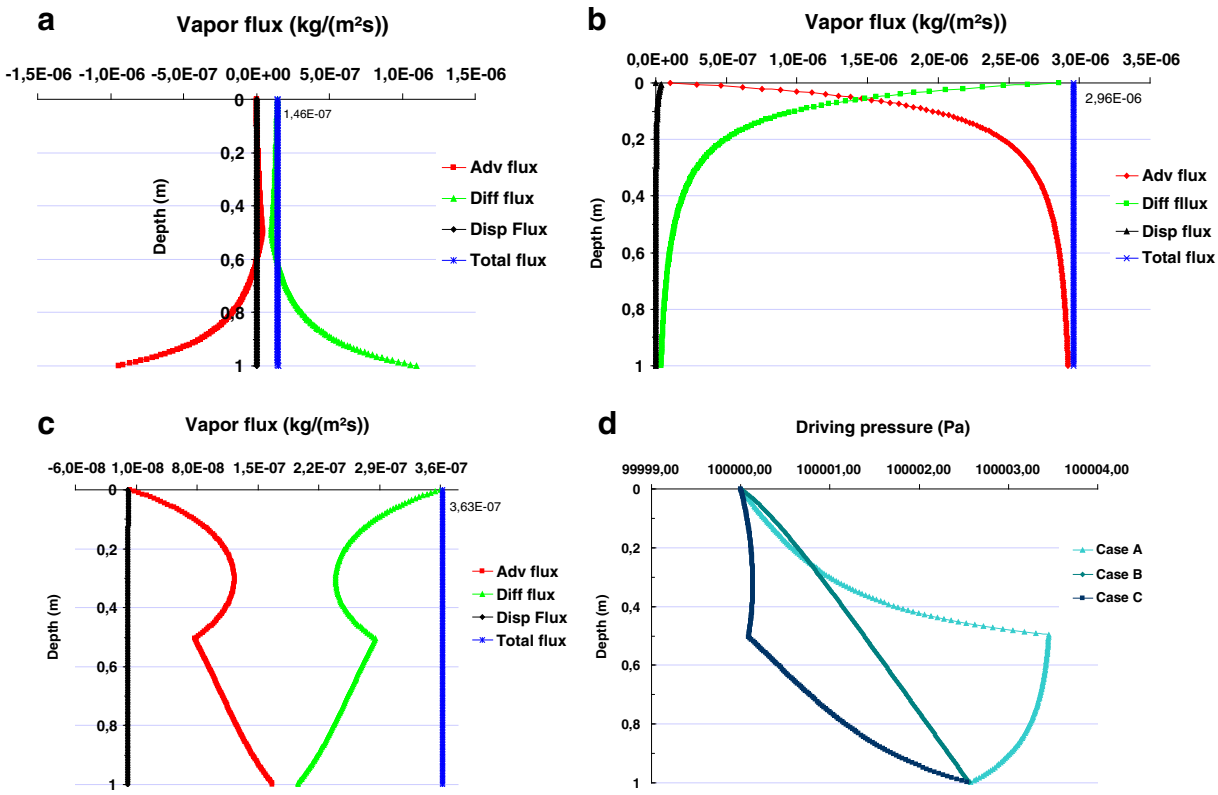

Fig. 9 Diffusive, dispersive, advective and total fluxes calculated in the *z*-direction for Run 4 at steady state for **a** cases A, **b** B, and **c** C, and **d** driving pressure calculated at steady state for Run 4 for cases A, B and C

the high vapour pressure prescribed at the upstream boundary, vapour transport is dominated by advection, and thus, after a short time, the entire soil column is saturated with the upstream vapour concentration.

It is worthwhile to note that, for the different runs, the vapour concentration at a given depth evolves proportionally with the overpressure prescribed at the upstream boundary of the soil column. The lower the overpressure, the lower the calculated vapour concentration will be.

4 Detailed Error Analysis

To quantify the total vapour flux leaving the soil column at the soil/atmosphere interface, a quasi-analytical approach is used. Using the database of the three case studies, two types of quasi-analytical approach are employed to predict the vapour flux at the soil surface and to quantify the error associated with these approaches.

4.1 Diffusion-Based Quasi-Analytical Approach (Approach 1)

The first approach is based on Fick's first law and describes the steady-state diffusive flux of vapour in the vertical *z*-direction per surface unit $F_{\mathrm{diff},\,z}$ (in kilogrammes per square metre per second) at a given point by

$$F_{diff,z} = -D_{eg}\frac{\partial C_a}{\partial z} \tag{14}$$

where D_{eg} (in square metres per second) denotes the effective diffusion coefficient and C_{a} (in kilogrammes per cubic metre) is the DNAPL vapour concentration at a given elevation. The mathematical formulation of D_{eg} is obtained from Eqs. (12) and (13):

$$D_{eg} = 0.66\frac{\theta_g^2}{n}D_g \tag{15}$$

Approaching the vertical concentration gradient in Eq. (14) by a finite difference formulation, the first quasi-analytical approach is obtained (Jellali et al.

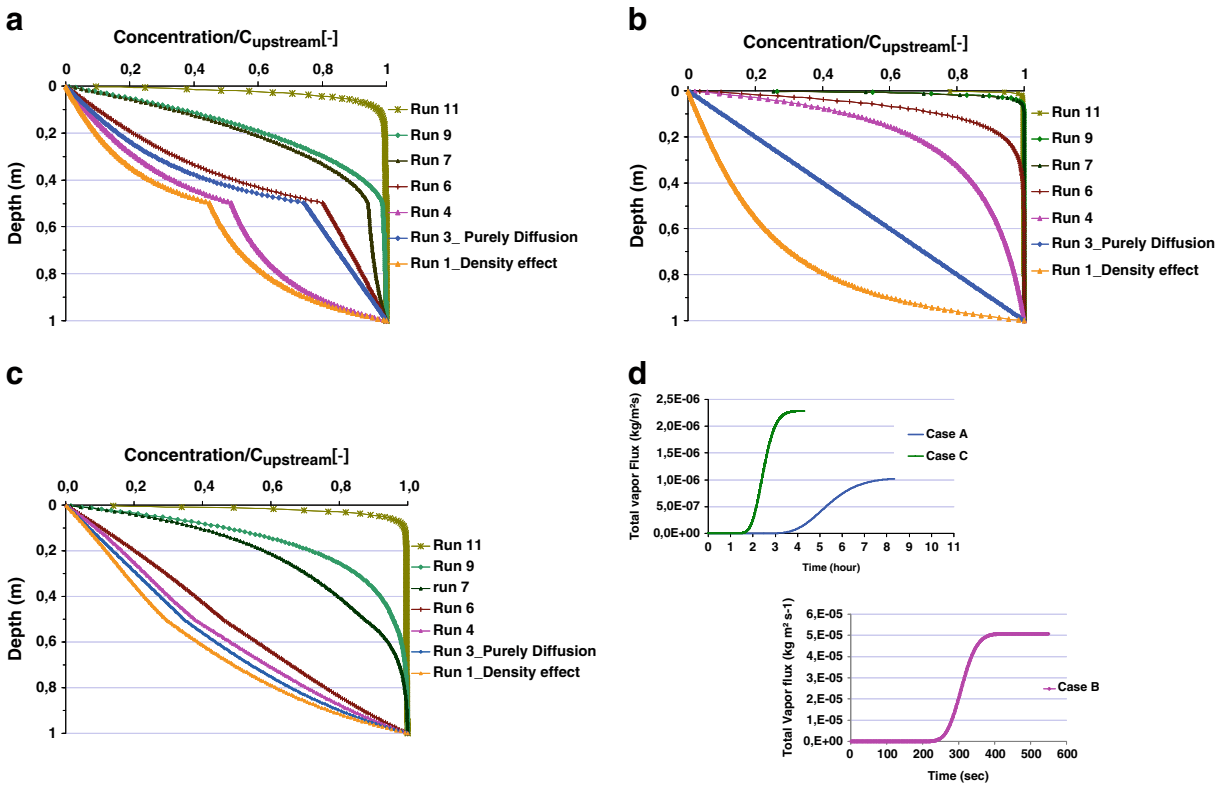

Fig. 10 Normalised vapour concentration calculated at steady state for Runs 1, 3, 4, 6, 7, 9 and 11 for **a** cases A, **b** B and **c** C, and **d** the total vapour fluxes calculated at the soil surface in Run 11 for cases A, B and C

2003; Dridi and Schäfer 2006), which predicts the vertical vapour flux at the soil surface to the atmosphere

$$F_{diff,z} = -\widetilde{D}_{eg}\frac{\Delta C_a}{\Delta \bar{z}} \equiv F_{loc,z} \tag{16}$$

where ΔC_a (in kilogrammes per cubic metre), defined as $\Delta C_a = C_a(z_2) - C_a(z_1)$, is the concentration difference between two points located at a vertical distance $\Delta\bar{z}$ (in metres), defined as $\Delta\bar{z} = z_2 - z_1$. In our study, one of the two selected points is placed on the soil surface ($z=0$). $\widetilde{D}_{eg}$ (in square metres per second) represents the average of the effective diffusion coefficient calculated using the arithmetic mean of the two effective diffusion coefficients determined at the two depths.

4.2 Diffusion–Dispersion–Advection-Based Quasi-Analytical Approach (Approach 2)

The second approach is mainly based on Fick's and Darcy's laws. At steady-state transport conditions, the total vertical flux $F_{tot,z}$ (in kilogrammes per square metre per second) in the unsaturated soil column is equal to the sum of the diffusive flux $F_{diff,z}$ (in kilogrammes per square metre per second), the dispersive flux $F_{disp,z}$ (in kilogrammes per square metre per second) and the advective flux $F_{adv,z}$ (in kilogrammes per square metre per second) in the vertical z-direction:

$$F_{tot,z} = F_{diff,z} + F_{disp,z} + F_{adv,z} \tag{17}$$

The diffusive flux $F_{diff,z}$ is expressed by Eq. (14).

Using a Fickian-based approach, the dispersive flux $F_{disp,z}$ (in kilogrammes per cubic metre) is given by

$$F_{disp,z} = -\alpha_L |v_{f,z}| \frac{\partial C_a}{\partial z}, \tag{18}$$

where α_L (in metres) is the longitudinal dispersivity of the porous medium, C_a (in kilogrammes per cubic metre) is the DNAPL vapour concentration at a given depth and $v_{f,z}$ (in metre per second) represents the specific discharge of the gaseous phase in the vertical direction, expressed by Darcy's law:

$$v_{f,z} = -\frac{k\rho g}{\mu}\frac{\partial h}{\partial z} \tag{19}$$

where h (in metres) is the pneumatic head. Applying the expression of the equivalent water pressure head introduced by Lusczynski (1960) to the pneumatic head (Cotel et al. 2011), it can be expressed as follows:

$$h \equiv \frac{p_g}{\rho_{air} g} = \frac{p_a}{\rho_{air} g} + z \tag{20}$$

The Darcy velocity in the z-direction can thus be expressed by

$$v_{f,z} = \frac{-k_{ra} k^* \rho_{air} g}{\mu_a} \left(\frac{\partial h}{\partial z} + \frac{\rho_a - \rho_{air}}{\rho_{air}} \right) \tag{21}$$

where p_g (in Pascals) is the driving pressure, p_a (in Pascals) is the pressure of the gas mixture (soil air/DNAPL vapour) at elevation z, g (in metres per square second) is the gravitational constant, μ_a (in Pascals times second) represents the dynamic viscosity, k_{ra} (−) is the relative gas permeability in biphasic system water/gas, ρ_{air} (in kilogrammes per cubic metre) is the density of the uncontaminated soil air and ρ_a (in kilogrammes per cubic metre) is the density of the gas mixture (soil air/DNAPL vapour).

The density of the gas mixture is given by:

$$\rho_a = C_a \left(1 - \frac{M_{air}}{M_{DNAPL}} \right) + \rho_{air} \tag{22}$$

M_{air} (in grammes per mole) is the molar mass of soil air and is equal to 28.9 g/mol, M_{DNAPL} (in grammes per mole) is the molar mass of the DNAPL and C_a (in kilogrammes per cubic metre) is the vapour concentration.

The advective flux in the vertical direction is given by

$$F_{adv,z} = v_{f,z} C_a \tag{23}$$

The total vapour flux can thus be quantified by

$$F_{tot,z} = \left(-D_{eg} - \alpha_L \left| \left(-\frac{k_{ra} k^* \rho_{air} g}{\mu_a} \left[\frac{\partial h}{\partial z} + \frac{\rho_a - \rho_{air}}{\rho_{air}} \right] \right) \right| \right) \frac{\partial C_a}{\partial z} + \left(-\frac{k_{ra} k^* \rho_{air} g}{\mu_a} \left[\frac{\partial h}{\partial z} + \frac{\rho_a - \rho_{air}}{\rho_{air}} \right] \right) C_a \tag{24}$$

Replacing the spatial derivatives by a finite difference formulation, the second quasi-analytical method is obtained:

$$F_{tot,z} \equiv F_{loc,z} = \left(-\widetilde{D}_{eg} - \widetilde{\alpha}_L \left| \left(-\frac{\widetilde{k_{ra}} \widetilde{k^*} \rho_{air} g}{\mu_a} \left[\frac{\Delta h}{\Delta \bar{z}} + \frac{\widetilde{\rho_a - \rho_{air}}}{\rho_{air}} \right] \right) \right| \right) \frac{\Delta C_a}{\Delta \bar{z}} + \left(-\frac{\widetilde{k_{ra}} \widetilde{k^*} \rho_{air} g}{\mu_a} \left[\frac{\Delta h}{\Delta \bar{z}} + \frac{\widetilde{\rho_a - \rho_{air}}}{\rho_{air}} \right] \right) \widetilde{C}_a \tag{25}$$

where $\widetilde{C}_a$, $\widetilde{k^*}$, $\widetilde{k}_{ra}$, $\widetilde{\rho}_a$ and $\widetilde{\alpha}_L$ represent the arithmetic averages between the two measuring points separated by $\Delta \bar{z}$ (in metres) and located on the same vertical direction and Δh (in metres), defined as $\Delta h = h(z_2) - h(z_1)$, is the pneumatic head difference. The selection of this type of mean is justified from the measuring conditions of real sites. Indeed, the concentration and pressure measurements might be available only at two points located near the soil surface.

4.3 Relative Errors

To analyse in detail the bias introduced by both the diffusion-based quasi-analytical approach and the diffusion–dispersion–advection-based quasi-analytical approach, we used the definition of the relative error between the local vapour flux, $F_{loc,z}$, calculated from the quasi-analytical approaches and the numerically calculated surface flux at the upper boundary of the soil column, $F_{surf,z}$, between the first two cells near the soil surface, considered as the reference value:

$$\delta = \frac{F_{loc,z} - F_{surf,z}}{F_{surf,z}} \tag{26}$$

The errors obtained using the diffusion-based quasi-analytical approach (see Eq. 16) are termed δ_{diff}, those obtained from the diffusion–dispersion–advection-based quasi-analytical approach (see Eq. 25) are termed $\delta_{diff-adv}$.

4.4 Predicted Vapour Fluxes Under Steady-State Conditions

4.4.1 Influence of Density-Driven Advection

In the following section, the concentration and pressure data of Run 1 at steady-state transport conditions are used to analyse the relative errors introduced by the two quasi-analytical approaches. Figure 11 plots

the quantified relative error as a function of the distance between the two points considered $\Delta\bar{z}$, for case studies A, B and C.

Case A For short vertical distances between the two measuring points, the relative errors calculated by both approaches are very small at approximately 0.003 because density effects are negligibly small up to a depth of 50 cm; near the soil surface, the total vertical vapour fluxes can thus be predicted using the diffusive flux.

By neglecting the effect of density in approach 1, the error δ_{diff} increases when $\Delta\bar{z}$ increases. The real vapour flux is overestimated by a factor of 1.2 when $\Delta\bar{z}$ is higher than 50 cm. Indeed, this result is directly linked to the given high vapour concentrations in the lower layer of case study A. Using only vertical concentration gradients without taking into account the negative advective flux induced by the density of the vapours will thus lead to a high overestimation of the real vapour fluxes at the soil surface at steady-state conditions.

Assuming that vapour diffusion is the only transport mechanism, an apparent effective diffusion coefficient D'_{eg} can be quantified (Fig. 12) by applying Fick's law (Eq. 14). To obtain the same low vapour flux at the soil surface as given in the database, D'_{eg} must be three times lower than the effective diffusion coefficient $\widetilde{D}_{eg}$ used in approach 1.

However, using approach 2, the maximum error does not exceed 30 % (Fig. 11a). Moreover, once the maximum is reached at $\Delta\bar{z}$=0.5 m, the error decreases considerably. As expected, approach 2 allows an appropriate prediction of the vapour flux at the soil surface.

Case B In the case of a homogeneous medium, approaches 1 and 2 accurately predict the vapour flux at the soil surface when the vertical measuring distance is small. As in case A, the density effect of vapour concentration is negligibly small as the high vapour concentrations are accumulated at the lower boundary of the soil column. Therefore, the apparent effective diffusion coefficient D'_{eg} using approach 1 is quite close to the effective diffusion coefficient $\widetilde{D}_{eg}$, and the quantified relative error ε is low (see Fig. 12b).

When $\Delta\bar{z}$ increases, the errors of the two approaches increase as the density effect is more significant in the lower part of the soil column. The relative error ε increases up to 70 %, corresponding to a D'_{eg} that must be three times lower than $\widetilde{D}_{eg}$ (see Fig. 12b).

For approach 2, the quantified error $\delta_{\text{diff–adv}}$ is negligible for vertical distances of up to 80 cm. When measuring point 2 is located at a depth of 80 cm or more, the vapour flux calculated using Eq. (25) underestimates the vapour flux at the soil surface given in the database by a factor of 2. This result is mainly due to the average vapour density between the two measuring points, which is based on an arithmetic mean that strongly overestimates the effect of the concentration field at the deeply located measuring point 2 when $\Delta\bar{z}$ increases.

Case C The steady-state vapour flux of case C given at the soil surface is better predicted by approach 2 than by approach 1. When measuring point 2 is placed near the soil surface, the quantified relative error δ of approach 2 is approximately 0.003, compared with 0.01 obtained using approach 1. Up to a vertical distance of 15 cm, the error $\delta_{\text{diff–adv}}$ of approach 2 does not exceed 2 %, whereas δ_{diff} reaches 10 % in approach 1. For vertical distances higher than 15 cm, the quantified relative errors increase due to the heterogeneous concentration and pressure field and may be positive or negative. At the layer interface, a discontinuity of errors δ_{diff} and $\delta_{\text{diff–adv}}$ appears of approximately −23 and 19 %, respectively (see Fig. 11c). As expected, approach 2 provides better estimates of the total vapour fluxes at the soil surface than approach 1.

4.4.2 Combined Influence of Density-Driven Advection and Pressure-Gradient-Induced Advection

In the following section, the concentration and pressure data of Run 4 at steady-state transport conditions are used to analyse the relative errors introduced by the two quasi-analytical approaches. Figure 13 plots the quantified relative error as a function of the distance between the two points considered $\Delta\bar{z}$ for case studies A, B and C.

As already described in Section 3.4.2, the slight overpressure added in Run 4 generated advective vapour fluxes caused by the gradient of driving pressure that dominate the mass fluxes caused by the vapour density in the studied homogenous soil (case B). However, in the layered soils (cases A and C), the overpressure selected at the upstream boundary does not have a predominant influence on the vertical mass flux of vapour. In these cases, vapour transport is affected by both the vapour density and the gradient of the driving pressure.

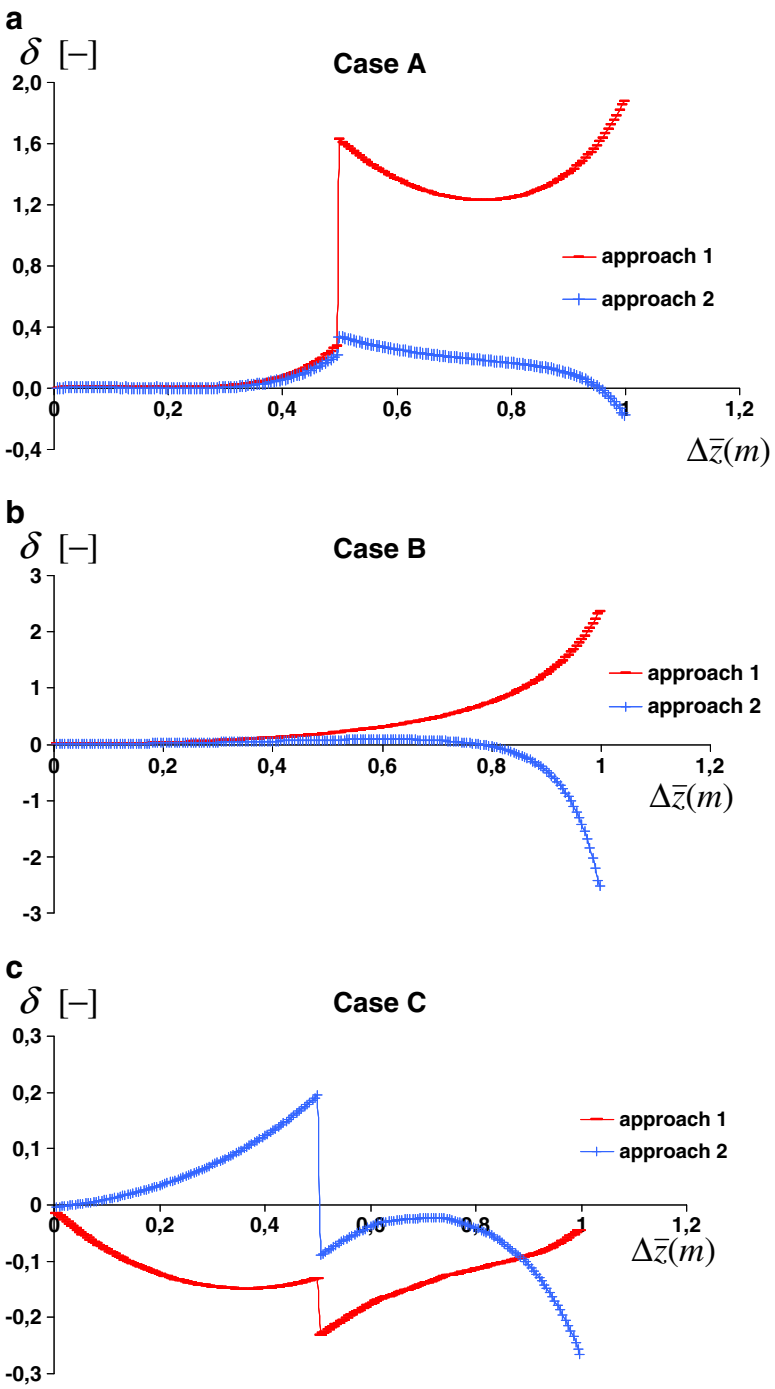

Fig. 11 Relative error as a function of the distance between the two points $\Delta\bar{z}$ for vapour density-driven induced advection (Run 1) at steady-state transport conditions for: **a** case studies A, **b** B and **c** C

Without taking into account the advective flux induced by the overpressure in the quasi-analytical approach, the relative error δ_{diff} (see Fig. 13) is negative, indicating an underestimate of the vapour flux at the soil surface in cases B and C. In case study B, the maximum relative error δ_{diff} reaches 88 % when $\Delta\bar{z}$ increases, as the diffusive vapour flux is negligible compared with the advective vapour flux caused by the vertical vapour pressure gradient.

Applying the quasi-analytical approach 2 to the database of case studies A and C, the error $\delta_{diff-adv}$ does not exceed 0.5 % as long as measuring point 2 is

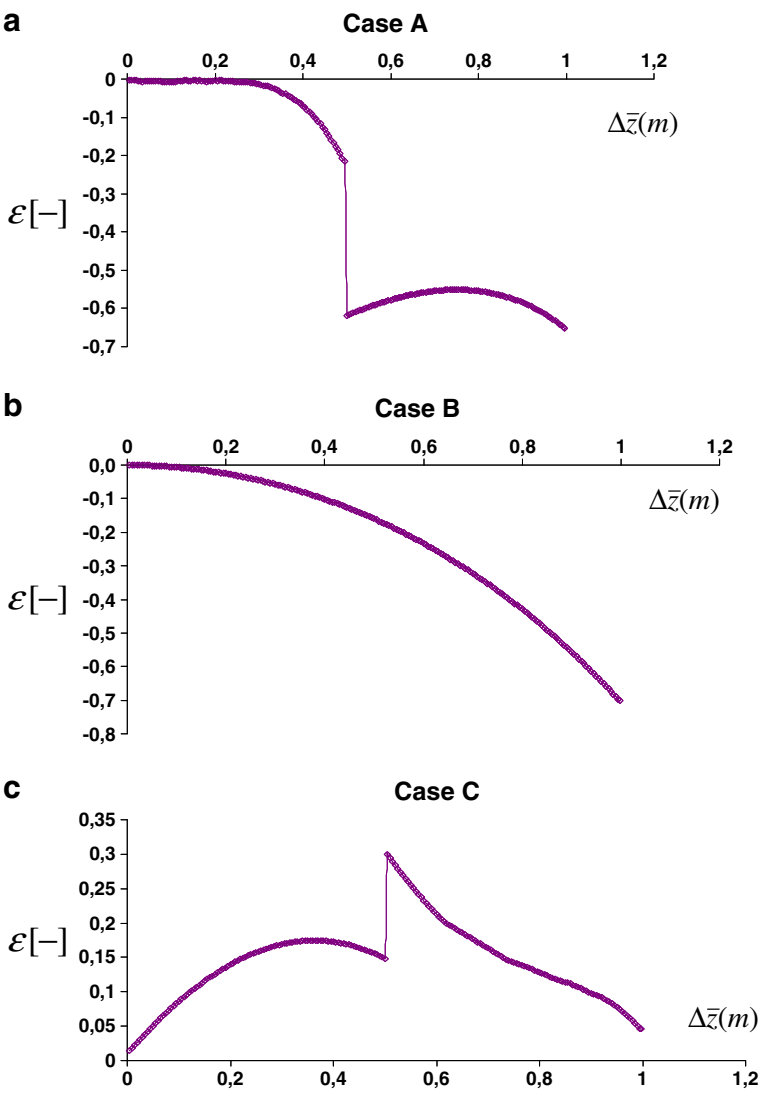

Fig. 12 Relative error of the effective diffusion coefficient determined from approach 1, $\varepsilon = \left(D'_{eg} - \widetilde{D}_{eg}\right)\Big/\widetilde{D}_{eg}$, as a function of the distance between the two points $\Delta\bar{z}$ based on the database of Run 1 at steady-state transport conditions for case studies A (**a**), B (**b**) and C (**c**)

placed near the soil surface. Up to a depth of 50 cm, the error $\delta_{\text{diff–adv}}$ remains constant and does not exceed 8 % for cases A and C or 30 % for case B. Approach 2 provides significantly better estimates of total vapour fluxes at the soil surface than approach 1.

However, once measuring point 2 is placed at a depth deeper than the layer discontinuity, the relative error increases significantly with increasing $\Delta\bar{z}$. The maximum error is 750 and 150 % in soil column A and soil column C, respectively. However, in the homogeneous soil column (case B), the relative error remains nearly constant along the column. Let us analyse in more detail these relative errors of column A for vertical distances of $\Delta\bar{z}$ higher than 50 cm. With increasing vapour pressure prescribed at the upstream boundary of the soil column (Runs 6, 9 and 11), the relative error $\delta_{\text{diff–adv}}$ increases (see Fig. 13d). This result is caused by both the averaging process of the transport parameters of the quasi-analytical approach, which are taken as the mean values between the two different soil textures, and the vapour pressure gradient. This explains why the highest relative errors are obtained in Run 11 when measuring point 2 is located at a depth of 50 cm or more.

It is worthwhile to note that the relative error δ_{diff} calculated for Run 6 is the smallest one. This result can be explained by the fact that the vertical TCE vapour profile at steady state is very close to that generated in Run 3, which represents the case of purely diffusive vapour transport (see Fig. 10a).

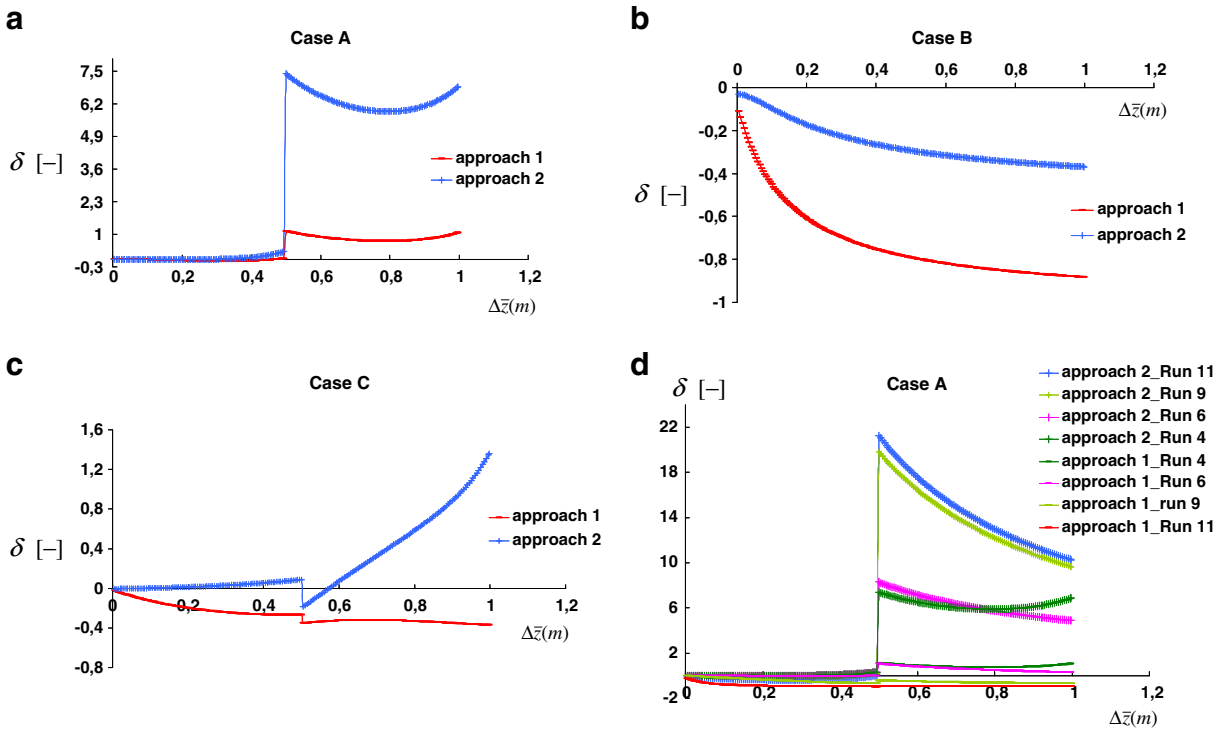

Fig. 13 Relative error as a function of the distance between the two points $\Delta\bar{z}$ in the case of combined influence of density-driven advection and pressure-gradient advection (Run 4) at steady-state transport conditions for **a** case studies A, **b** B, and **c** C, and **d** relative errors at steady state for case A for Runs 4, 6, 9 and 11

5 Conclusions

The transport mechanisms of TCE vapours in partially water-saturated soil columns were studied under various flow and transport boundary conditions. The concentration and pressure database used was created for three different soil textures using a coupled numerical flow and transport model.

The obtained results confirm the findings of Cotel et al. (2011) that density-driven advection of TCE vapours may be a significant transport mechanism in natural soils. Indeed, when the soil column was subjected to high vapour concentrations without significantly increased vapour pressures, the dominant transport mechanism was advection caused by the vapour density effect. In this case characterised by a uniform water content profile, the TCE vapour concentration is accumulated at the bottom of the homogeneous soil column after 1.5 days. However, in a layered soil structure with highly non-uniform water content, DNAPL vapours may migrate more significantly towards the soil surface. The intrinsic permeability is an important parameter that significantly influences the vertical vapour concentration profile. The lower the intrinsic permeability, the lower the dimensionless Rayleigh number and density effect will be. This result is consisted with the findings of Cotel et al. (2011). However, the position of the fine sand layer greatly affects the total vapour flux leaving the soil column at the soil surface, strongly reducing the diffusive vapour mass flux when the effective gas diffusion coefficients are low due to the high water content. In general, for vapour concentrations lower than one tenth of the DNAPL saturation concentration, the effect of vapour density may be neglected, and the vapour concentration profile is dominated by molecular diffusion.

The results of the conducted studies indicate that small driving pressure gradients resulting from local overpressure in the soil gas may create a significant ascendant vapour movement towards the soil surface. For the homogeneous soil column, the steady-state vapour concentration profile was characterised by normalised concentrations higher than 0.5 occupying 90 % of the soil column height. Steady-state transport conditions were reached in the homogeneous medium-

sized sand in only few minutes, whereas the presence of layer discontinuities significantly increased the time required to reach steady state.

A detailed analysis was performed to quantify the errors introduced from two quasi-analytical approaches to evaluate the steady-state flux of vapours at the soil surface when the concentration profiles are strongly influenced by density-driven and pressure gradient-induced advection.

The relative errors associated with the quantification of the vapour fluxes at the soil surface were observed to depend on the dominant transport mechanisms, the evaluation of the vapour concentration and pressure in the porous medium and the selected quasi-analytical approach. Dridi and Schäfer (2006) revealed that the relative error can also depend on the transport regime and the average value of the dimensionless Henry constant.

For predominantly density-driven advective transport, the local mass flux calculated by the quasi-analytical approach 1 (based on Fick's first law) is quite close to the given surface flux of cases A and B. This approach only slightly overestimates the real fluxes within the order of several percentages when the vertical distance between the two measurement points is less than 50 cm. Above this limit, the error increases significantly when increasing the vertical distance. Without taking into account the density effect, the apparent effective gaseous diffusion coefficient derived at the bottom of the soil column must be three times lower than the real effective diffusion coefficient to fit the mass flux given at the soil surface. Conversely, using the quasi-analytical approach 2 (based on Fick's first and Darcy's laws), the error becomes very small for almost all vertical distances. When driving pressure gradients become significant, the vapour fluxes calculated using the second approach are rather close to the vapour flux given at the soil surface when the vertical distance between the two measuring points is lower than 50 cm. Beyond the layer discontinuity, this approach systematically overestimates the vapour flux at the soil surface in cases A and C. This result is mainly caused by the heterogeneity of the soil and overpressure selected at the upstream boundary. The higher the vapour overpressure, the higher the relative errors calculated by approach 2.

In all of the studied cases with driving pressure gradients in the soil gas, the influence of longitudinal dispersion on the total vertical vapour flux was negligibly small compared with that of molecular diffusion. Neglecting the dispersive mass flux in quasi-analytical approach 2 is thus justified and simplifies its application in field cases. It is worthwhile to note that in field cases, density-driven advection and pressure-gradient-induced advection may simultaneously appear and represent dominant transport mechanisms. In this case, the quasi-analytical approach 2 permits the prediction of steady-state vapour fluxes at the soil surface with only a small bias.

Appendix A

The flow of soil air is given by the mass conservation equation, which contains mass flux divergence and variation of storage terms as a function of time:

$$-\nabla(\rho v) = \frac{\partial(n\rho)}{\partial t} \tag{27}$$

where ρ (in kilogrammes per cubic metre) is the vapour density, v (in metres per second) is the Darcy's velocity and n (−) the porosity of the porous media.

The storage term can be explained as follows:

$$\frac{\partial(n\rho)}{\partial t} = n\frac{\partial\rho}{\partial t} + \rho\frac{\partial n}{\partial t} \tag{28}$$

Many assumptions are considered to express the flow equation. The first one is to assume that if the compressibility of the medium $\frac{\partial n}{\partial t}$ is negligible compared with the gas compressibility $\frac{\partial\rho}{\partial t}$, the storage term will be simplified and defined as follows:

$$\frac{\partial(n\rho)}{\partial t} = n\frac{\partial\rho}{\partial t} \tag{29}$$

Introducing the ideal gas state equation $\rho(p,T) = \frac{pM}{RT}$ into Eq. (29), the term of storage variation becomes equal to

$$n\frac{\partial}{\partial t}(\rho) = \frac{nM}{RT}\frac{\partial p}{\partial t} \tag{30}$$

where M (in kilogrammes per mole) is the molecular weight of the gas, p (in Pascals) is the pressure, R (8.314 $\mathrm{Pa\,m^3\,mol^{-1}\,K^{-1}}$) is the universal ideal gas constant and T (in Kelvins) is the absolute temperature.

In the divergence term, the velocity of the TCE vapour v is given by Darcy's law:

$$v = -\frac{k}{\mu}\nabla(\rho g z + p) \tag{31}$$

where k (in square metres) is the gas permeability, g (in metres per square second) is the gravity acceleration, μ (in kilogrammes per metre per second) is the dynamic viscosity of the fluid and z (in metres) is the elevation. The left-hand side term of Eq. (30) can thus be rewritten as:

$$-\nabla(\rho v) = -\nabla\left(-\frac{k\rho}{\mu}\nabla(\rho g z + p)\right) \tag{32}$$

$$-\nabla(\rho v) = \nabla\left(\frac{k\rho}{\mu} g z \nabla(\rho) + g\rho\nabla(z) + \nabla(p)\right) \tag{33}$$

$$= \nabla\left(\frac{k\rho}{\mu} g z \nabla\rho\right) + \nabla\left(\frac{k\rho}{\mu} g\rho\nabla z\right) + \nabla\left(\frac{k\rho}{\mu}\nabla p\right) \tag{34}$$

Assuming that variation of the vapour density $\rho(p, T)$ with elevation z is negligible compared with the variation with pressure (p) or temperature (T), one can neglect the first term of Eq. (34). Using the ideal gas state equation, Eq. (30) takes the following developed form:

$$-\nabla(\rho v) = \nabla\left(\frac{kM^2p^2}{\mu R^2T^2} g\right) + \nabla\left(\frac{kMp}{\mu RT}\nabla p\right) \tag{35}$$

M, g, R, T being constants, Eq. (35) can be rewritten:

$$-\nabla(\rho v) = \frac{M^2 g}{\mu R^2T^2}\nabla\left(kp^2\right) + \frac{M}{\mu RT}\nabla(kp\nabla p) \tag{36}$$

The term $p\nabla p$ may be replaced by

$$\left(p\frac{\partial p}{\partial z}\right) = \frac{1}{2}\left(p\frac{\partial p}{\partial z} + p\frac{\partial p}{\partial z}\right) = \frac{1}{2}\frac{\partial(p.p)}{\partial z} = \frac{1}{2}\frac{\partial p^2}{\partial z} \tag{37}$$

Using Eq. (37) in Eq. (36) leads to:

$$-\nabla(\rho v) = \frac{M^2 g}{\mu R^2T^2}\frac{\partial}{\partial z}\left(kp^2\right) + \frac{M}{2\mu RT}\frac{\partial}{\partial z}\left(k\frac{\partial p^2}{\partial z}\right) \tag{38}$$

Based on Eqs. (30) and (38), one can express the mass conservation equation (see Eq. 27) of 1D vertical gas flow in a porous medium based on pressure p:

$$\frac{nM}{RT}\frac{\partial p}{\partial t} = \frac{M^2 g}{\mu R^2T^2}\frac{\partial}{\partial z}\left(kp^2\right) + \frac{M}{2\mu RT}\frac{\partial}{\partial z}\left(k\frac{\partial p^2}{\partial z}\right) \tag{39}$$

To linearise Eq. (39), the term p^2 is replaced by p using the following expression:

$$\frac{\partial p^2}{\partial t} = \frac{\partial(p.p)}{\partial t} = p.\frac{\partial p}{\partial t} + p\frac{\partial p}{\partial t} = 2p.\frac{\partial p}{\partial t} \tag{40}$$

Replacing $\frac{\partial p}{\partial t}$ by $\frac{1}{2}\frac{\partial p^2}{p\,\partial t}$ in Eq. (39), one obtains

$$\frac{\partial p^2}{\partial t} = 2\frac{Mp}{n\mu RT} g\frac{\partial}{\partial z}\left(kp^2\right) + \frac{p}{n\mu}\frac{\partial}{\partial z}\left(k\frac{\partial}{\partial z}p^2\right) \tag{41}$$

As soil gas may occupy only a part of the given pore volume, one must replace porosity n by the gas content θ_g, leading to the following equation:

$$\frac{\partial p^2}{\partial t} = \frac{p}{\mu\theta_g}\frac{\partial}{\partial z}\left(k\frac{\partial p^2}{\partial z}\right) + 2\frac{Mgp}{\mu RT\theta_g}\frac{\partial}{\partial z}\left(kp^2\right) \tag{42}$$

To simplify the notation of Eq. (42), one sets $P=p^2$ and finally obtains:

$$\frac{\partial P}{\partial t} = \beta\frac{\partial}{\partial z}\left(k\frac{\partial P}{\partial z}\right) + 2\gamma\frac{\partial}{\partial z}(kP) \tag{43}$$

where $\beta = \frac{P_0}{\mu\theta_g}$, $\gamma = \frac{MgP_0}{\mu RT\theta_g}$ and p_0 represents the initial pressure in the soil gas.

Appendix B

The integrals of the linearised flow equation (Eq. 8) are defined as follows:

$$\int_{k-1/2}^{k+1/2}\frac{\partial P}{\partial t}dz = \int_{k-1/2}^{k+1/2}\beta\frac{\partial}{\partial z}\left(k\frac{\partial P}{\partial z}\right)dz + \int_{k-1/2}^{k+1/2}2\gamma\frac{\partial}{\partial z}(kP)dz \tag{44}$$

Using an implicit time scheme (discretisation at time $t+1$), the integrals for cell k can be expressed as:

$$P_{k-1}^{t+1}GP(k) + P_k^{t+1}EP(k) + P_{k+1}^{t+1}FP(k) = P_k^t \tag{45}$$

where

$$EP(k) = [1 + \beta^k\frac{\Delta t}{\Delta z^2}k^{k-1/2} + \beta^k\frac{\Delta t}{\Delta z^2}k^{\,k+1/2} - \gamma^k\frac{\Delta t}{\Delta z}k^{k+1/2} + \gamma^k\frac{\Delta t}{\Delta z}k^{k-1/2}] \tag{46}$$

$$FP(k) = \left[-\beta^k \frac{\Delta t}{\Delta z^2} k^{k+1/2} - \gamma^k \frac{\Delta t}{\Delta z} k^{k+1/2}\right] \tag{47}$$

$$GP(k) = \left[-\beta^k \frac{\Delta t}{\Delta z^2} k^{k-1/2} + \gamma^k \frac{\Delta t}{\Delta z} k^{k-1/2}\right] \tag{48}$$

GP(k) is the factor accounting for the mass flux in the upstream cell $k-1$, EP(k) is a factor representing the mass flux in cell k and FP(k) is mass flux in the downstream cell $k+1$.

Eq. (45) is given in matrix form as follows:

$$\begin{pmatrix}
EP(1) & FP(1) & 0 & 0 & 0 & 0 & 0 & 0 & 0 & 0 \\
GP(2) & EP(2) & FP(2) & . & . & & & 0 & 0 & 0 \\
. & . & . & . & . & . & . & . & 0 & 0 & 0 & 0 \\
. & . & . & . & . & . & . & . & & & & \\
0 & & & & & & & & & & & \\
0 & & & & & & & & & & & \\
. & . & . & . & . & . & . & & & & & 0 \\
. & . & . & . & . & . & . & & & & & 0 \\
. & . & . & . & . & . & \ldots & .. & 0 & 0 & 0 \\
\ldots & GP(NCELL\text{-}1) & EP(NCELL\text{-}1) & FP(NCELL\text{-}1) & & & & & & & & \\
. & . & . & . & . & . & GP(NCELL) & EP(NCELL) & & & &
\end{pmatrix}
\begin{pmatrix} P_1^{t+1} \\ P_2^{t+1} \\ . \\ . \\ . \\ P_{NCELL-1}^{t+1} \\ P_{NCELL}^{t+1} \end{pmatrix}
=
\begin{pmatrix} P_1^t + GP(1)P_{upstream} \\ P_2^t \\ . \\ . \\ . \\ . \\ P_{NCELL-1}^t \\ P_{NCELL}^t \end{pmatrix}$$

where

$$EP(1) = \left[1 + 2\beta^1 \frac{\Delta t}{\Delta z^2}\kappa^1 + \beta^1 \frac{\Delta t}{\Delta z^2}\kappa^2 - \gamma^1 \frac{\Delta t}{\Delta z}\kappa^2 + \gamma^1 \frac{\Delta t}{\Delta z}\kappa^1\right] \tag{49}$$

$$FP(1) = \left[-\beta^1 \frac{\Delta t}{\Delta z^2} k^2 - \gamma^1 \frac{\Delta t}{\Delta z} k^2\right] \tag{50}$$

$$GP(1) = \left[-2\beta^1 \frac{\Delta t}{\Delta z^2} k^1 + \gamma^1 \frac{\Delta t}{\Delta z} k^1\right] \tag{51}$$

and

$$EP(NCELL) = \left[\begin{array}{r} 1 + \beta^{NCELL} \frac{\Delta t}{\Delta z^2} k^{NNODE-1} + 2\beta^{NCELL} \frac{\Delta t}{\Delta z^2} k^{NNODE} \\ - \gamma^{NCELL} \frac{\Delta t}{\Delta z} k^{NNODE} + \gamma^{NCELL} \frac{\Delta t}{\Delta z} k^{NNODE} \end{array}\right] \tag{52}$$

$$GP\,(NCELL) = \left[-\beta^{NCELL} \frac{\Delta t}{\Delta z^2} k^{NNODE} + \gamma^{NCELL} \frac{\Delta t}{\Delta z} k^{NNODE}\right] \tag{53}$$

The same approach was used to numerically solve the transport equation (Eq. 10):

$$\int_{k-1/2}^{k+1/2} \alpha \frac{\partial C}{\partial t} dz = \int_{k-1/2}^{k+1/2} \frac{\partial}{\partial z}\left[D_{eg} + \alpha_L |v|\right] \frac{\partial C}{\partial z} dz + \int_{k-1/2}^{k+1/2} -\frac{\partial}{\partial z}(vC) dz \tag{54}$$

Using an implicit time scheme, one obtains:

$$C_{k-1}^{t+1} G(k) + C_k^{t+1} E(k) + C_{k+1}^{t+1} F(k) = C_k^t \tag{55}$$

where

$$G(k) = \left[\frac{\left(D_{eg}^{k-1/2} + \alpha_L^k v^{k-1/2}\right)\Delta t}{\alpha^k \Delta z^2} - \frac{v^{k-1/2}\Delta t}{\alpha^k \Delta z}\right] \tag{56}$$

$$E(k) = \left[1 + \frac{\left(D_{eg}^{k-1/2} + \alpha_L^k v^{k-1/2}\right)\Delta t}{\alpha^k \Delta z^2} + \frac{\left(D_{eg}^{k+1/2} + \alpha_L^k v^{k+1/2}\right)\Delta t}{\alpha^k \Delta z^2} + \frac{v^{k+1/2}\Delta t}{\alpha^k \Delta z}\right] \tag{57}$$

$$F(k) = \left[-\frac{\left(D_{eg}^{k+1/2} + \alpha_L^k v^{k+1/2}\right)\Delta t}{\alpha^k \Delta z^2}\right] \tag{58}$$

Equation (56) can be written in matrix form as follows

$$\begin{pmatrix} E(1) & F(1) & 0 & \cdots & 0 & 0 & 0 & 0 \\ G(2) & E(2) & F(2) & \cdots & 0 & 0 & 0 & 0 \\ \cdots & \cdots & \cdots & \cdots & \cdots & \cdots & \cdots & \cdots \\ 0 & 0 & 0 & \cdots & G(NCELL-1) & E(NCELL-1) & F(NCELL-1) & \\ 0 & 0 & 0 & 0 & 0 & \cdots & 0 & G(NCELL) \quad E(NCELL) \end{pmatrix} \begin{pmatrix} c_1^{t+1} \\ c_2^{t+1} \\ \cdots \\ c_{NCELL}^{t+1} \end{pmatrix} = \begin{pmatrix} c_1^t - c_{upstream} G(1) \\ c_2^t \\ \cdots \\ c_{NCELL-1}^t \\ c_{NCELL}^t \end{pmatrix}$$

Where

$$G(1) = \left[-2 \frac{\left(D_{eg}^1 + \alpha_L^1 v^1 \right) \Delta t}{\alpha^1 \Delta z^2} - \frac{v^1 \Delta t}{\alpha^1 \Delta z^2} \right] \tag{59}$$

$$E(1) = \left[1 - 2 \frac{\left(D_{eg}^1 + \alpha_L^1 v^1 \right) \Delta t}{\alpha^1 \Delta z^2} - \frac{\left(D_{eg}^2 + \alpha_L^1 v^2 \right) \Delta t}{\alpha^1 \Delta z^2} + \frac{v^2 \Delta t}{\alpha^1 \Delta z^2} \right] \tag{60}$$

$$F(1) = \left[\frac{\left(D_{eg}^2 + \alpha_L^1 v^2 \right) \Delta t}{\alpha^1 \Delta z^2} \right] \tag{61}$$

and

$$G(NCELL) = \left[\frac{\left(D_{eg}^{NNODE} + \alpha_L^{NCELL} v^{NNODE} \right) \Delta t}{\alpha^{NCELL} \Delta z^2} - \frac{v^{NNODE} \Delta t}{\alpha^{NCELL} \Delta z} \right] \tag{62}$$

$$E(NCELL) = \left[1 - \frac{\left(D_{eg}^{NNODE} + \alpha_L^{NCELL} v^{NNODE} \right) \Delta t}{\alpha^{NCELL} \Delta z^2} - 2 \frac{\left(D_{eg}^{NNODE+1} + \alpha_L^{NCELL} v^{NNODE+1} \right) \Delta t}{\alpha^{NCELL} \Delta z^2} + \frac{v^{NNODE+1} \Delta t}{\alpha^{NCELL} \Delta z} \right] \tag{63}$$

References

Altevogt, A. S., Rolston, D. E., & Venterea, R. T. (2003). Density and pressure effects on the transport of gas phase chemicals in unsaturated porous media. *Water Resources Research, 39*(3), 1061.

Barber, C., Davis, G. B., Briegel, D., & Ward, J. K. (1990). Factors controlling the concentration of methane and other volatiles in groundwater and soil gas around a waste site. *Journal of Contaminant Hydrology, 5*, 155–169.

Bear, J. (1972). *Dynamics of fluids in porous media*. New York: Elsevier.

Benremita, H. (2002). *Approche expérimentale et simulation numérique du transfert de solvants chlorés en aquifère alluvial contrôlé*. Thèse de doctorat, Université Louis Pasteur, Strasbourg. France

Benremita, H., & Schäfer, G. (2003). Quantification du transfert de trichloroéthylène en milieu poreux à partir d'un panache de vapeurs vers la nappe d'eau souterraine. *C.R. Mécanique, 331*(12), 835–842.

Bettahar, B., Ducreux, J., Schäfer, G., & Van Dorpe, V. (1999). Surfactant enhanced in situ remediation of LNAPL contaminated aquifers: large scale studies on a controlled experimental site. *Transport in Porous Media, 37*, 276–286.

Birovljev, A., Furuberg, L., Feder, J., Jøssang, T., Måløy, K. J., & Aharony, A. (1991). Gravity invasion percolation in 2 dimensions-experiment and simulation. *Physical Review Letters, 5*, 584–587.

Bohy, M., Schäfer, G., & Razakarisoa, O. (2004). Caractérisation de zones sources de DNAPL à l'aide de traceurs bisolubles: mise en évidence d'une cinétique de partage. *C.R. Géoscience, 336*, 799–806.

Bohy, M., Dridi, L., Schäfer, G., & Razakarisoa, O. (2006). Transport of mixture of chlorinated solvent vapours in the vadoses zone of a sandy aquifer. *Vadose Zone Journal, 5*, 539–553.

Choi, J. W., Tillman, F. D., & Smith, J. A. (2002). Relative importance of gas phase diffusive and advective trichloroethylene fluxes in the unsaturated zone under natural conditions. *Environmental Science and Technology, 36*, 3157–3164.

Coppola, A., Kutilek, M., & Frind, E. O. (2009). Transport in preferential flow domains of the soil porous system: measurement, interpretation, modelling and upscaling. *Journal of Contaminant Hydrology, 104*, 1–3.

Cotel, S. (2008). *Etude des transferts sol/nappe/atmosphère/bâtiments; application aux sols pollués par des Composés Organiques Volatils*. Ph.D. thesis, University of Joseph Fourier, Grenoble, France

Cotel, S., Schäfer, G., Barthes, V., & Baussand, P. (2011). Effect of density-driven advection on trichloroethylene vapour diffusion in a porous medium. *Vadose zone Journal, 10*, 565–581.

Direction Régionale de Santé Publique (DRSP). (2007). Etude sur l'intrusion potentielle de vapeurs de trichloréthylène dans l'air intérieur des bâtiments du secteur Valcartier, Québec. http://www.dspq.qc.ca/documents/1_021007_AVIS_TCE_000.pdf. Accessed May 2009.

Dridi, L., & Schäfer, G. (2006). Quantification du flux de vapeurs de solvants chlorés depuis une source en aquifère poreux vers l'atmosphère: biais relatifs à la non uniformité de la teneur en eau et à la non stationnarité du transfert. *C. R. Mecanique, 334*, 611–620.

Dridi, L., Pollet, I., Razakarisoa, O., & Schäfer, G. (2009). Characterisation of a DNAPL source zone in a porous aquifer using the partitioning interwell tracer test and an inverse modelling approach. *Journal of Contaminant Hydrology, 107*, 22–44. doi:0.1016/j.jconhyd.2009.03.003.

Falta, R. W., Javandel, I., Pruess, K., & Witherspoon, P. A. (1989). Density-driven flow of gas in the unsaturated zone due to the evaporation of volatile organic compounds. *Water Resources Research, 25*, 2159–2169.

Fayers, F. J., & Zhou, D. (1996). On the importance of gravity and three-phase flow in gas displacement processes. *Journal of Petroleum Science and Engineering, 15*, 321–341.

Grathwohl, P. (1998). *Diffusion in natural porous media: contaminant transport, sorption/desorption and dissolution kinetics*. Dordrecht: Kluwer Academy Publication.

Hodgson, A. T., Garbesi, K., Sextro, R. G., & Daisy, J. M. (1992). Soil-gas contamination and entry of volatile organic compounds into a house near a landfill. *Journal of the Air and Waste Management Association, 42*, 277–283.

Jang, W. Y., & Aral, M. M. (2007). Density-driven transport of volatile organic compounds and its impact on contaminated groundwater plume evolution. *Transport in Porous Media, 67*(3), 353–374.

Jellali, S., Benremita, H., Muntzer, P., Razakarisoa, O., & Schäfer, G. (2003). A large-scale experiment on mass transfer of trichloroethylene from the unsatured zone of a sandy aquifer to its interfaces. *Journal of Contaminant Hydrology, 60*, 31–53.

Jones, C. J., Hudson, B. C., McGugan, P. J., & Smith, A. J. (1978). The leaching of some halogenated organic compounds from domestic waste. *Journal of Hazardous Materials, 2*(3), 227–233.

Johnson, P. C., & Ettinger, R. A. (1991). Heuristic model for predicting the intrusion rate of contaminant vapours into buildings. *Environmental Science and Technology, 25*, 1445–1452.

Kram, M. L., Keller, A. A., Rossabi, J., & Everett, L. G. (2001). DNAPL characterization methods and approaches, part 1: performance comparisons. *Ground Water Monitoring and Remediation, 21*, 109–123.

Kueper, B. H., & Frind, E. O. (1989). An overview of immiscible fingering in porous media. *Journal of Contaminant Hydrology, 2*, 95–110.

Lenhard, R. J., Oostrom, M., Simmons, C. S., & White, M. D. (1995). Investigation of density-dependent gas advection of trichloroethylene: experiment and a model validation exercise. *Journal of Contaminant Hydrology, 19*, 47–67.

Lusczynski, N. J. (1960). Head and flow of ground water of variable density. *Journal of Geophysical Research, 66*, 4247–4256.

Mastrocicco, M., Colombani, N., & Petitta, M. (2011). Modelling the density contrast effect on a chlorinated hydrocarbon plume reaching the shore line. *Water, Air, and Soil Pollution, 220*(1–4), 387–398.

Mendoza, C. A., & Frind, E. O. (1990). Advective–dispersive transport of dense organic vapours in the unsaturated zone, 1, model development. *Water Resources Research, 26*, 379–387.

Mendoza, C. A., & McArly, T. A. (1990). Modeling of groundwater contamination caused by organic solvents vapours. *Ground Water, 28*, 199–206.

Moldrup, P., Olesen, T., Rolston, D. E., & Yamaguchi, T. (1997). Modeling diffusion and reaction in soil: VII. Predicting gas and ion diffusivity in unsaturated and sieved soil. *Soil Science, 162*, 632–640.

Molins, S., Mayer, K. U., Amos, R. T., & Bekins, B. A. (2010). Vadose zone attenuation of organic compounds at a crude oil spill site interactions between biogeochemical reactions and multicomponent gas transport. *Journal of Contaminant Hydrology, 112*(1–4), 15–29.

Morrison, G., Zhao, P., & Kasthuri, L. (2006). Spatial considerations in the transport of pollutants to indoor surfaces. *Atmospheric Environment, 40*(20), 3677–3685.

Nordstrom, D. K., & Munoz, J. L. (1985). *Geochemical thermodynamics*. Menlo Park: The Benjamin/Cummings Publishing Co., Inc.

Pankow, J. F., & Cherry, J. A. (1996). *Dense chlorinated solvents and other DNAPLs in groundwater: history, behaviour and remediation*. Ontario: Waterloo Press.

Parker, J. C. (2003). Physical processes affecting natural depletion of volatile chemicals in soil and groundwater. *Vadose Zone Journal, 2*, 222–230.

Perry, R. H., & Green, D. W. (1984). *Perry's chemical engineer's handbook* (p. 2336). New York: McGraw-Hill.

Rivett, M. O., Wealthall, G. P., Dearden, R. A., & McAlary, T. A. (2011). Review of unsaturated-zone transport and attenuation of volatile organic compound (VOC) plumes leached from shallow source zones. *Journal of Contaminant Hydrology, 123*, 130–156.

Schwille, F. (1988). *Dense chlorinated solvents in porous and fractured media model experiments. Transcrit par Pankow J. F., English Language Edition*. Chelsea: Lewis Publishers.

Sililo, O. T. N., & Tellam, J. H. (2000). Fingering in unsaturated zone flow: a qualitative review with laboratory experiments on heterogeneous systems. *Ground Water, 38*(6), 864–871.

Sleep, B. E., & Sykes, J. F. (1989). Modeling the transport of volatile organics in variably saturated media. *Water Resources Research, 25*, 81–92.

Thiez, A., & Ducreux, J. (1994). A 3-D numerical model for analysing hydrocarbon migration into soils and aquifers. In Siriwardane & Zaman (Eds.), *Computer methods and advances in geomechanics* (pp. 1165–1170). Rotterdam: Balkema.

Thomson, N. R., Sykes, J. F., & Van Vliet, D. (1997). A numerical investigation into factors affecting gas and aqueous phase plumes in the subsurface. *Journal of Contaminant Hydrology, 28*(1–2), 39–70.

Waitz, M. F. W., Freijer, J. I., Kreule, P., & Swartjes, F. A. (1996). *The VOLASOIL risk assessment model based on CSOIL for soils contaminated with volatile compounds. RIVM report no. 715810014*. Bilthoven: National Institute of Public Health and the Environment (RIVM).

Wang, G., Reckhorn, S. B. F., & Grathwohl, P. (2003). Volatilization of VOC from multicomponent mixtures in unsaturated porous media. *Vadose Zone Journal, 2*, 692–701.

Webb, S. W., & Pruess, K. (2003). The use of Fick's law for modeling trace gas diffusion in porous media. *Transport in Porous Media, 51*, 327–341.

White, M. D., Oostrom, M., Rockhold, M. L., & Rosing, M. (2008). Scalable modeling of carbon tetrachloride migration at the Hanford Site using the STOMP simulator. *Vadose Zone Journal, 7*(2), 654–666.

Williams, G. M., Ward, R. S., & Noy, D. J. (1999). Dynamics of landfill gas migration in unconsolidated sands. *Waste Management and Research, 17*, 1–16.

Yu, S., Unger, A. J. A., & Parker, B. (2009). Simulating the fate and transport of TCE from groundwater to indoor air. *Journal of Contaminant Hydrology, 107*, 140–161.